Science of the Total Environment 974 (2025) 179190

Contents lists available at ScienceDirect

Science of the Total Environment

journal homepage: www.elsevier.com/locate/scitotenv

Validation of GEMS operational v2.0 total column NO_2 and HCHO during the GMAP/SIJAQ campaign

Kangho Bae [a,b], Chang-Keun Song [a,b,c,*], Michel Van Roozendael [d], Andreas Richter [e], Thomas Wagner [f], Alexis Merlaud [d], Gaia Pinardi [d], Martina M. Friedrich [d], Caroline Fayt [d], Ermioni Dimitropoulou [d,1], Kezia Lange [e], Tim Bösch [e], Bianca Zilker [e], Miriam Latsch [e], Lisa K. Behrens [e], Steffen Ziegler [f], Simona Ripperger-Lukosiunaite [f], Leon Kuhn [f], Bianca Lauster [f], Lucas Reischmann [f], Katharina Uhlmannsiek [f], Alexander Cede [g], Martin Tiefengraber [g], Manuel Gebetsberger [g], Rokjin J. Park [h], Hanlim Lee [i], Hyunkee Hong [j], Lim-Seok Chang [j], Kwonho Jeon [j]

[a] Department of Civil, Urban, Earth and Environmental Engineering, Ulsan National Institute of Science and Technology (UNIST), Ulsan, Republic of Korea
[b] Research & Management Center for Particulate Matters at the Southeast Region of Korea, Ulsan National Institute of Science and Technology (UNIST), Ulsan, Republic of Korea
[c] Graduate School of Carbon Neutrality, Ulsan National Institute of Science and Technology (UNIST), Ulsan, Republic of Korea
[d] Royal Belgian Institute for Space Aeronomy BIRA-IASB, Brussels, Belgium
[e] Institute of Environmental Physics, University of Bremen, Bremen, Germany
[f] Max-Planck Institute for Chemistry, Mainz, Germany
[g] Luftblick, Innsbruck, Austria
[h] School of Earth and Environmental Sciences, Seoul National University, Seoul, Republic of Korea
[i] Division of Earth Environmental System Science, Major of Spatial Information Engineering, Pukyong National University, Busan, Republic of Korea
[j] Environmental Satellite Center, National Institute of Environmental Research, Incheon, Republic of Korea

HIGHLIGHTS

- A comparative analysis of MAX-DOAS and Pandora was investigated.
- GEMS total column NO_2 and HCHO was validated using Pandora and MAX-DOAS measurements in South Korea.
- A significant overestimation of GEMS NO_2 data was observed, particularly in urban areas like Seoul, compared to rural areas.
- A systematic underestimation of GEMS HCHO total column product was observed, particularly in large columns.

GRAPHICAL ABSTRACT

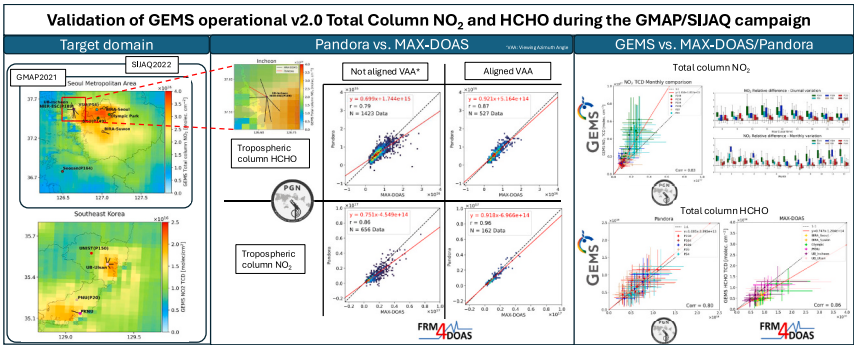

* Corresponding authors at: Research & Management Center for Particulate Matters at the Southeast Region of Korea, Department of Civil, Urban, Earth and Environmental Engineering, Graduate School of Carbon Neutrality, Ulsan National Institute of Science & Technology (UNIST), 50 UNIST-gil, Ulju-gun, Ulsan 689-798, Republic of Korea.
E-mail address: cksong@unist.ac.kr (C.-K. Song).
[1] Now at Royal Meteorological Institute RMI, Brussels, Belgium.

https://doi.org/10.1016/j.scitotenv.2025.179190
Received 6 October 2024; Received in revised form 18 March 2025; Accepted 19 March 2025
Available online 25 March 2025
0048-9697/© 2025 The Authors. Published by Elsevier B.V. This is an open access article under the CC BY-NC-ND license (http://creativecommons.org/licenses/by-nc-nd/4.0/).

ARTICLE INFO

Editor: Hongliang Zhang

Keywords:
GEMS
MAX-DOAS
Pandora
Validation
GMAP/SIJAQ
Diurnal variation

ABSTRACT

The Geostationary Environmental Monitoring Spectrometer (GEMS), the first geostationary air quality instrument, onboard the GEO-KOMPSAT-2B (GK2B) satellite, produces hourly observations over Asia with 3.5 km × 8 km spatial resolution. To evaluate the GEMS L2 products, the National Institute of Environmental Research (NIER) organized the GEMS Map of Air Pollutants 2021 (GMAP2021) and the Satellite Integrated Joint monitoring of Air Quality 2022 (SIJAQ2022) campaigns during October 2021 to November 2021 and from June 2022 to July 2022, respectively. While GMAP2021 mainly targeted the SMA (Seoul Metropolitan Area), the SIJAQ2022 campaign extended to the southeastern area of South Korea. In this study, a comparison between Pandora and Multi-AXis Differential Optical Absorption Spectroscopy (MAX-DOAS) products and an evaluation of the GEMS operational v2.0 total column NO_2 and HCHO products are conducted.

A comparative analysis between the Pandora (P189) and the IUP Bremen MAX-DOAS instrument at the Incheon NIER-ESC site was performed to analyze discrepancies between the retrieval processors (Pandora: PGN official processor, MAX-DOAS: MMF in FRM_4DOAS framework). Aligning the viewing directions of both Pandora and MAX-DOAS leads to a significant increase in the slope and correlation coefficient from 0.87 to 0.96 and from 0.86 to 0.96, respectively, in the case of NO_2 tropospheric columns. Similarly, for HCHO tropospheric columns, slope and correlation coefficient change from 0.94 to 1.09 and from 0.81 to 0.90 when matching the viewing geometries of both instruments. In contrast to tropospheric columns, total HCHO columns derived from Pandora (P189) direct-sun measurements show significantly larger values than the MAX-DOAS ones, with a mean relative difference (MRD) of 126 %. This bias can however be reduced to 33 % after suitable adjustment of the direct-sun retrieval settings.

The GEMS v2.0 NO_2 total column product, evaluated over 6 official PGN sites in South Korea, shows good agreement with a correlation coefficient of 0.87 and similar seasonal and diurnal NO_2 variation. However, GEMS tends to report higher values than Pandora with a mean relative difference of +41 %. The magnitude of the GEMS overestimation is amplified in highly polluted conditions (i.e. during winter and at noontime).

Compared to 6 MAX-DOAS stations and 6 Pandora stations, the GEMS HCHO product captures well the seasonal and diurnal variation of HCHO and shows good agreement both with MAX-DOAS and Pandora with slopes of 0.84 and 0.79, respectively, and correlation coefficients of 0.86 for both. Large columns, however, tend to be systematically underestimated.

1. Introduction

Nitrogen oxides ($NO_x = NO + NO_2$) are key species for air quality research due to their toxicity and significant role in atmospheric chemistry. NO_x is mainly emitted as NO, which quickly converts to NO_2 by reacting with ozone (O_3). NO_x is naturally emitted from sources such as soil, lightning, and natural biomass burning. In recent decades, the emissions of NO_x have dramatically increased due to anthropogenic sources including domestic heating (Schiavon et al., 2015; Ozgen et al., 2021), power plants (Kim et al., 2006; Saw et al., 2021), transportation (Jaeglé et al., 2005; Kousoulidou et al., 2008), and industrial activities (Van Der et al., 2008). High-concentrations of NO_2 directly cause respiratory diseases such as asthma, lung cancer, and cardiopulmonary condition (Elsayed, 1994; Eum et al., 2022) and it contributes to the formation of particulate matter (PM) (Behera and Sharma, 2011; Chu et al., 2020). In addition, NO_2 is a key component controlling ozone production through reactions involving Volatile Organic Compounds (VOCs) (Crutzen, 1979; Haagen-Smit, 1952). Due to its high reactivity, the lifetime of NO_2 in the lower atmosphere is only a few hours (Laughner and Cohen, 2019).

Formaldehyde (HCHO) is another important trace gas in atmospheric chemistry. HCHO is an intermediate product of the VOCs oxidation and can be considered as a tracer of VOCs (Li et al., 2014; Lui et al., 2017). The background concentration of HCHO mainly results from the oxidation of methane (CH_4) (González Abad et al., 2016) but higher concentrations are found over continents due to direct emissions from industrial sources as well as the oxidation of non-methane volatile organic compounds (NMVOCs) emitted by human activity and biogenic sources (Dutta et al., 2010). HCHO is a carcinogen, and can cause inspiratory diseases and headaches (EPA, 2015; Zhu et al., 2017a). Furthermore, HCHO is a key reactant in tropospheric ozone chemistry, as photochemical reactions produce hydroperoxyl radicals (HO_2), which subsequently reacts with nitric oxide (NO) to produce hydroxyl radicals (OH). Due to its high reactivity, the lifetime of HCHO is just a few hours in the atmosphere (De Smedt et al., 2008).

Due to their short lifetimes, the spatial distributions of both NO_2 and HCHO are closely related to the location of their emission sources, which has been used to estimate emission fluxes (Beirle et al., 2011; de Foy et al., 2015; Ghude et al., 2008; Gonzi et al., 2011). Space-borne instruments such as the Global Ozone Monitoring Experiment (GOME; Burrows et al., 1999 and GOME-2; Munro et al., 2006), the SCanning Imaging Absorption spectrometer for Atmospheric CartograpHY (SCIAMACHY; Bovensmann et al., 1999), the Ozone Monitoring Instrument (OMI; Levelt et al., 2006), the Ozone Mapping and Profiler Suite (OMPS; Flynn et al., 2006) and the TROPOspheric Monitoring Instrument (TROPOMI; Veefkind et al., 2012), all operated on polar orbit satellites (Low-Earth Orbit; LEO), have been used since the mid-nineties providing valuable information on NO_2 and HCHO spatial distributions and trends with full-earth coverage (Richter et al., 2005; Schneider et al., 2015; Van Der et al., 2006; Zhu et al., 2017b). Since they overpass a target region in mid latitudes only once or twice a day at best, LEO satellites are limited in their temporal coverage. To overcome this limitation and inform on the diurnal characteristics of atmospheric trace gas concetrations, Korea launched the first geostationary environmental monitoring satellite GEMS (Geostationary Environmental Monitoring Spectrometer) in 2020 (Kim et al., 2020). This was followed by the US TEMPO (Tropospheric Emissions: Monitoring of Pollution) mission launched in 2023 (Zoogman et al., 2017) and, in 2025, the European Space Agency (ESA) will launch the Copernicus Sentinel-4 instrument (Gulde et al., 2017).

For the validation of GEMS measurements, the National Institute of Environmental Research (NIER) has been expanding the Pandora network over Asia by organizing the PAN (Pandora Asia Network). Furthermore, NIER organized two successive international field campaigns GMAP (GEMS Map of Air Pollution) and SIJAQ (Satellite Integrated Joint monitoring of Air Quality) during autumn 2021 and summer 2022.

Kim et al. (2023) evaluated the GEMS operational v1.0 NO_2 vertical column density (VCD) products using four Pandora instruments from November 2020 to January 2021 in Seosan, Korea. This study reported that the GEMS v1.0 NO_2 VCD product was lower than Pandora

observations and showed correlation coefficients of 0.62–0.78. Lange et al. (2024) evaluated the tropospheric NO_2 VCD from the GEMS operational v2.0 processor and the IUP-UB scientific product using Pandora and MAX-DOAS data during the GMAP and SIJAQ campaigns. The GEMS operational product overestimated ground-based instruments by a median relative bias of 64 % with a correlation coefficient of 0.75. In contrast, the IUP-UB scientific product showed a median relative bias of −1 % with a correlation coefficient of 0.82. This study found that urban areas exhibit maximum NO_2 columns around 11 LST, while rural areas show nearly no diurnal variability. Lee et al. (2024) conducted the first evaluation of the GEMS operational v2.0 HCHO product using Fourier-Transform Infrared (FTIR) and Multi-AXis Differential Optical Absorption Spectroscopy (MAX-DOAS) from October 2020 to January 2021 in Xianghe, China. They found that the GEMS HCHO product was 30–40 % lower than MAX-DOAS and FTIR observations, likely due to differences in vertical sensitivity between the instruments. Applying an averaging kernel smoothing method reduced this low bias by about 10–15 %. Nevertheless, GEMS effectively captured the seasonal variability of HCHO over East Asia.

In sections 2 and 3, we briefly introduce the GMAP and SIJAQ campaigns conducted over Korea, as well as the satellite and ground-based remote sensing data used in this study. In section 4, focusing on the NIER-ESC site, comparison results of NO_2 and HCHO retrievals obtained by MAX-DOAS and Pandora instruments are presented. The validation of GEMS operational v2.0 NO_2 and HCHO total column products using Pandora and MAX-DOAS instruments operated over Korea is reported in Section 5.

2. GMAP/SIJAQ campaigns

The GMAP/SIJAQ campaigns are a set of field campaigns organized in Korea by NIER. One of their main objectives was to perform intensive field measurements to produce a reference data set for validating the GEMS retrieval products based on surface in-situ, in-situ aircraft, airborne remote sensing, car DOAS, and stationary remote sensing observations. The GMAP2021 campaign (https://www.sijaq.org/home, last access: 25 March 2024) took place from October 2021 to November 2021 over the Seoul Metropolitan Area (SMA). Subsequently, from June 2022 to August 2022, the SIJAQ2022 campaign (https://sijaq2.sijaq.org/, last access: 25 March 2024) was conducted by expanding the target domain to the southeastern area of Korea which includes the cities of Busan and Ulsan.

In the beginning of the GMAP2021 campaign, early October 2021, the Royal Belgian Institute for Space Aeronomy (BIRA-IASB), the Institute of Environmental Physics, University of Bremen (IUP Bremen), and the Max Planck Institute for Chemistry (MPIC) installed three MAX-DOAS instruments at the rooftop of NIER-ESC for one week intercomparison, before each instrument moved to a different observation site (BIRA_Suwon, UB_Incheon, MPIC_Olympic, respectively, see Table 1). Details on the intercomparison experiment can be found in Van Roozendael et al. (2024). UB_Incheon and MPIC_Olympic sites were continuously operated until mid-November 2022 and early August 2022, respectively. BIRA-IASB operated the BIRA-Suwon station during the GMAP2021 campaign period, then moved to the BIRA-Seoul site from December 2021 to June 2022. For SIJAQ2022, IUP Bremen and MPIC installed additional MAX-DOAS instruments at UB_Ulsan and MPIC_PKNU in Ulsan and Busan respectively. In addition to the MAX-DOAS instruments from the European groups, 6 official PGN Pandora stations were also involved in the campaign. Furthermore, NIER installed two additional non-PGN Pandora instruments. To ensure optimal consistency, this study only uses official data that were calibrated and processed by the PGN processors. The location and information of all sites used in this study are described in Fig. 1 and Table 1. The operational periods of each instrument are illustrated in Fig. A.1 and the observation schedule of GEMS can be found in Fig. A.2.

3. Instruments

3.1. MAX-DOAS

The Multi-axis Differential Optical Absorption Spectroscopy (MAX-DOAS) is a ground-based remote sensing technique used for observing trace gases in the atmosphere such as NO_2, SO_2, and HCHO (Hönninger et al., 2004). MAX-DOAS instruments conduct vertical scanning at multiple elevation angles from 0° to 90°. In general, NO_2 and HCHO profiles can be reliably retrieved from near the ground up to approximately 2 km altitude. Vertical columns are representative of the column between the surface and 4 km of altitude (Irie et al., 2011; Tirpitz et al., 2021). The differential slant column densities (dSCDs) are fitted from a set of off-axis spectra and a corresponding reference zenith spectrum. The dSCDs are converted to VCDs by applying the Air Mass Factor (AMF) (Platt and Stutz, 2008). In this campaign, we processed spectra obtained from each instrument using first QDOAS (Danckaert et al., 2017) to get the dSCD and then the Mexican MAX-DOAS Fit (MMF; Friedrich et al., 2019) algorithm for retrieving tropospheric VCDs. The analysis was performed using the centralized FRM_4DOAS framework (https://frm4doas.aeronomie.be, last access: 12 March 2024). The quality flagging of MMF as implemented in the FRM_4DOAS framework takes into account the degree of freedom (DOF) of the retrieval, the root mean square (RMS) of the difference between measured and simulated dSCD and a stability criterion based on using different a priori values for the aerosol retrieval. Three quality flag values are possible: 2 (quality check failed), 1 (warning) and 0 (ok). The FRM_4DOAS framework provides quality flags independently from both the MMF and Mainz profile algorithm (MAPA, Beirle et al., 2019), as well as an overall quality flag by combining the quality flags from both algorithms. In our analysis, we only consider MMF retrieved data filtered with overall quality flags (qa_flag_no2 and qa_flag_hcho) of 0 and 1.

3.2. Pandora

The Pandora instrument is a hyperspectral UV–visible ground-based

Table 1
Geolocation information and observation period of stationary instrument sites.

Instrument	Station	Affiliation	Location	Period
MAX-DOAS	BIRA_Seoul	BIRA-IASB	Seoul (127.026° E, 37.585° N)	2021.12.19–2022.06.02
MAX-DOAS	BIRA_Suwon	BIRA-IASB	Suwon (127.010° E, 37.284° N)	2021.10.21–2021.12.16
MAX-DOAS	UB_Incheon	IUP-Bremen	Incheon (126.638° E, 37.569° N)	2021.10.09–2022.11.14
MAX-DOAS	UB_Ulsan	IUP-Bremen	Ulsan (129.306° E, 35.493° N)	2022.06.30–2022.11.13
MAX-DOAS	MPIC_Olympic	MPIC	Seoul (127.093° E, 37.503° N)	2021.10.19–2022.08.05
MAX-DOAS	PKNU	MPIC	Busan (129.107° E, 35.135° N)	2022.06.17–2022.08.10
Pandora 1S	P149	SNU	Seoul (126.951° E, 37.458° N)	2021.10.01–2022.11.30
Pandora 1S	P150	UNIST	Ulsan (129.190° E, 35.575° N)	2021.10.01–2022.11.03
Pandora 1S	P164	NIER	Seosan (126.494° E, 36.777° N)	2021.10.30–2022.11.30
Pandora 1S	P189	NIER	Incheon (126.638° E, 37.569° N)	2022.02.03–2022.11.30
Pandora 1S	P20	PNU	Busan (129.083° E, 35.235° N)	2021.10.01–2022.11.30
Pandora 1S	P54	YSU	Seoul (126.934° E, 37.564° N)	2021.10.01–2022.11.30

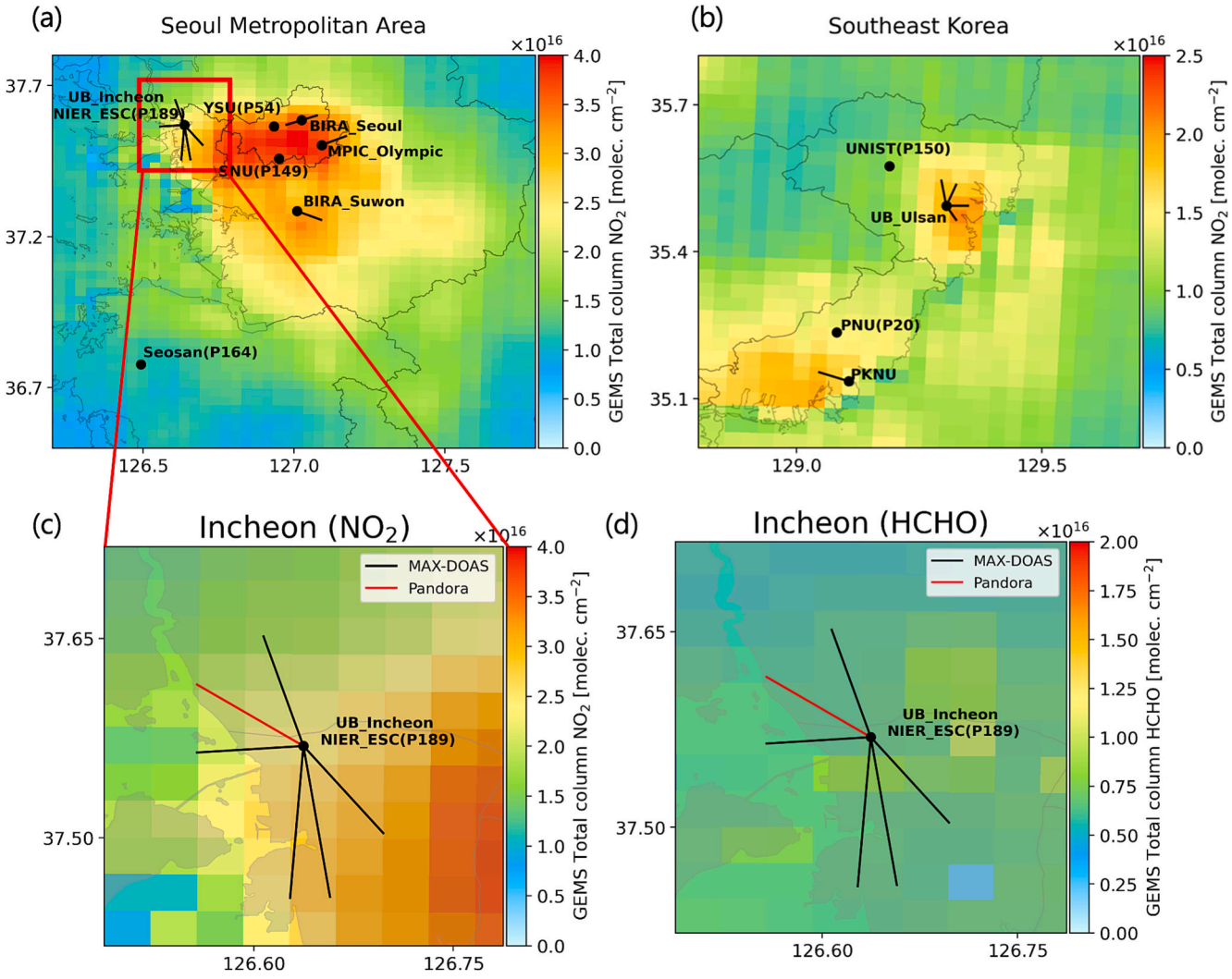

Fig. 1. Overview of the campaign domain and the location of stationary instruments over (a) the Seoul Metropolitan Area (SMA) and (b) the Southeast region. The background color represents the averaged GEMS total column NO_2 from October 2021 to November 2022. The black dot represents the location of each ground-based remote sensing instrument station, and the black lines are the viewing directions of each MAX-DOAS. (c) is a zoomed-in view of the Incheon region (red box) in (a), with the viewing direction of the MAX-DOAS (black) and Pandora (red). (d) is the same as (c), but the background color represents the averaged GEMS total column HCHO for the same period.

instrument that has a 280 nm to 530 nm spectral range and 0.6 nm spectral resolution (Herman et al., 2009). It was developed by NASA to fill the lack of ground-based trace gas observations. The Pandora observation network is maintained by the Pandonia-Global-Network (PGN), which involves a collaboration between NASA and ESA. Measurement data from Pandora instruments are automatically transferred to the PGN server and are centrally processed through the Blick Software Suite to retrieve L2 products. Official products are available via the PGN data server (https://data.pandonia-global-network.org/, last access: 22 March 2024). In addition to total column (TCD) products derived from direct-sun measurements, PGN also retrieves tropospheric columns and surface concentrations from sky measurements, using a technique similar to the MAX-DOAS one. The retrieval algorithms for total and tropospheric columns of NO_2 and HCHO are well described in Herman et al. (2009) and in Spinei et al. (2018), respectively. The HCHO TCD from Pandoras manufactured before summer 2019, including those used in Spinei et al. (2018), was affected by HCHO outgassing from Delrin parts in the sensor head, which made HCHO TCDs from direct-sun measurements unusable in hot environments (>28 °C) (Spinei et al., 2020). This issue was resolved by changing the hardware after summer of 2019. The Pandoras used in this research have been manufactured after summer 2019 and are therefore not affected.

In this paper, all Pandora data were processed with the Blick software version 1.8 (Cede, 2021) and retrieval version nvs3, nvh3, fus5 and fuh5 for total NO_2, tropospheric NO_2, total HCHO, and tropospheric HCHO VCD, respectively. The detailed description of the retrieval codes can be found in the PGN data product readme (https://www.pandonia-global-network.org/wp-content/uploads/2023/11/PGN_DataProducts_Readme_v1-8-8.pdf, last access: 2024.07.22). Additionally to fus5 for P189, we used a corrected HCHO TCD data set labeled fus7, where the background polynomial used in the spectral fitting was modified from 4th to 2nd order. In this research, we only use good (0, 10) and medium (1, 11) quality flags for all Pandora products.

3.3. GEMS

GEMS is a hyperspectral UV–visible imaging spectrometer that covers the spectral range of 200 to 500 nm with 0.6 nm spectral resolution. GEMS is onboard the GK2B (GEO-KOMPSAT 2B) satellite alongside GOCI-2 (Geostationary Ocean Color Imager-2), launched in February 2020.

Since its launch, GEMS has been continuously monitoring the air

quality over the Asian region (5S-45°N, 75E-145°E) with 3.5 km × 8 km spatial resolution (over Seoul) and an hourly (~ eight times per a day) temporal resolution (Kim et al., 2020). It provides information on vertical columns of NO_2, O_3, HCHO, and aerosols with original resolution. For the weak absorbers such as SO_2 and CHOCHO, pixels are co-added to increase the signal-to-noise ratio.

The retrieval of NO_2 is performed with the DOAS fitting algorithm within a 432–450 nm fitting window (Park et al., 2020), while HCHO is derived using the non-linearized fitting method of Basic Optical Absorption Spectroscopy (BOAS) (Chance et al., 2000) in a 329.3–358.6 nm fitting window (Kwon et al., 2019; Lee et al., 2024). In the BOAS method, dSCDs are directly determined by fitting the measured radiance using the nonlinear least squares inversion. The quality of the GEMS retrieval is assessed through flags, which are based on different criteria for each product. The NO_2 product employs a 3-bit binary structure, where each bit represents the good sample or not (0: use, 1: not use), a secondary summary quality flag (0: good, 1: have issue), and bad (not recommended for use). For HCHO, the quality of the retrieval is classified into seven categories: good (0), suspect (1), bad (2), good and suspect of gap-filled pixels (3, 4), missing (−1), and no-data (−999). Detailed description about the quality flags can be found in the GEMS User Guide (https://nesc.nier.go.kr/en/html/satellite/guide/guide.do, last access: 2025.01.16). It is recommended to use data with a final algorithm flag of 0 to ensure high accuracy.

In this research, GEMS operational v2.0 total column NO_2 and HCHO products (https://nesc.nier.go.kr/en/html/datasvc/index.do, last access: 24 December 2023) are validated. Only pixels with a cloud fraction of <0.33 and a final algorithm flag of 0 were used for evaluation. Additionally, to eliminate persistent outliers in the GEMS HCHO products, we removed unrealistic low ($< -2 \times 10^{16}$ molec. cm^{-2}) and large ($> 2 \times 10^{17}$ molec. cm^{-2}) values. Such extreme values deviate significantly from the range observed by ground-based instruments over the Korean Peninsula (-4×10^{15} to 7×10^{16} molec. cm^{-2}).

3.4. TROPOMI

TROPOMI is a nadir-viewing grating UV-VIS-NIR-SWIR spectrometer (UV: 270–320 nm, VIS: 310–500 nm, NIR: 675–775 nm, SWIR: 2305–2385 nm), onboard the Sentinel-5 Precursor satellite (Veefkind et al., 2012). TROPOMI was launched in October 2017 by ESA to support air quality and climate change research by monitoring gaseous pollutants such as CO, HCHO, CH_4, NO_2, O_3, SO_2, and aerosols. TROPOMI is passing over Korea ranged from 12:28–14:40 LST and its spatial resolution is 3.5 km × 5.5 km at nadir-view.

The TROPOMI total column (TCD) NO_2 operational product is retrieved from the DOAS spectral fitting method within a 405–465 nm range spectral window by the Royal Netherlands Meteorological Institute (KNMI) (van Geffen et al., 2022).

The HCHO product is also retrieved using DOAS fitting in the spectral window 328.5–359 nm. It uses daily updated reference spectra determined as mean spectra taken over the equatorial Pacific area a day before the measurement. The detailed description of the HCHO retrieval algorithm can be found in De Smedt et al. (2018).

In this research, we use RPRO and OFFL data processed with the v02.04 processor. The bad-quality pixels are removed with the recommended qa_value of under 0.75 for NO_2 (Eskes and Eichmann, 2023) and under 0.5 for HCHO (De Smedt et al., 2023). Additionally, we removed cloudy pixels with cloud_fraction_crb above 0.33 for both NO_2 and HCHO.

4. Comparison of Pandora and MAX-DOAS measurements

MAX-DOAS and Pandora instruments are commonly used for the validation of satellite data products (Dimitropoulou et al., 2020; Liu et al., 2023; Peters et al., 2012; Tzortziou et al., 2012, Pinardi et al., 2020., Verhoelst et al., 2021). However, as Pandora retrieves trace gases with the PGN algorithm, and the MAX-DOAS data used in this work were processed with the MMF algorithm as implemented in the FRM_4DOAS framework, there is a lack of comparative results between the L2 products retrieved by each class of instruments. This chapter conducts a comparative analysis of NO_2 and HCHO products retrieved using the MMF algorithm applied to IUP-Bremen MAX-DOAS data and the PGN processor applied to Pandora (P189). Both instruments were simultaneously operated on the rooftop of the National Institute of Environmental Research – Environmental Satellite Center (NIER-ESC) in Incheon from July 2022 to November 2022.

The viewing azimuth angles (hereafter, VAA) of MAX-DOAS and Pandora are illustrated in Fig. 1(c). The MAX-DOAS instrument performed sky elevation scans in 5 different VAAs (137.5°, 170°, 185°, 266.5°, and 340°), while the Pandora performed a combination of direct-sun and sky measurements at 300° VAA. To evaluate the effects of aligning the observational geometries of Pandora and MAX-DOAS, the comparison of tropospheric column products was conducted for 3 cases: (1) using MAX-DOAS data from all VAAs, (2) using MAX-DOAS data at 266.5° and 340° VAA, and (3) using the average values between 266.5° and 340° VAA (hereafter, 2-VAA averaged). A coincident measurement data set was created by averaging Pandora data within a 3 min window based on the MAX-DOAS scan time. The 2-VAA averaged MAX-DOAS value was calculated when the difference of observation times between measurements with VAA 266.5° and 340° was <15 min.

We calculate the slope and intercept parameters using a Reduced Major Axis (RMA) regression (Clarke, 1980), as well as mean difference (MD), mean relative difference (MRD), standard deviation, and correlation coefficient. MD is defined as the mean value of the difference between Pandora and MAX-DOAS (Eq. 1) and MRD is a normalized value of MD with MAX-DOAS (Eq. 2). These statistics are also used in section 5 by replacing $VCD_{Pandora}$ with VCD_{GEMS} and $VCD_{MAX-DOAS}$ with VCD_{Ground}

$$MD = \frac{1}{N}\sum_{i=1}^{N}\left(VCD_{Pandora,i} - VCD_{MAX-DOAS,i}\right) \quad (1)$$

$$MRD = \frac{1}{N}\sum_{i=1}^{N}\left(\frac{VCD_{Pandora,i} - VCD_{MAX-DOAS,i}}{VCD_{MAX-DOAS,i}}\right) \times 100\% \quad (2)$$

4.1. Pandora sky measurement vs MAX-DOAS

Comparison results from the different data sets described above are displayed in Fig. 2. Fig. 2(a) compares the tropospheric NO_2 VCDs from Pandora sky measurements at 300° VAA and IUP-Bremen MAX-DOAS data across all VAAs. We find a correlation coefficient of 0.86, however Pandora tropospheric NO_2 columns are lower than the MAX-DOAS columns with a slope of 0.87, a MD of -3.57×10^{15} molec. cm^{-2}, and a MRD of −28 %. The observed discrepancies might be due to the spatial inhomogeneity of NO_2 near the NIER-ESC site as shown in Fig. 1(c): the northwest region of the station, which coincides with the direction of Pandora sky measurements, shows lower NO_2 levels in average compared to the southeast. Consequently, during coincident observation period, the MAX-DOAS instrument observing at VAAs of 137.5°, 170°, and 185° is likely to measure higher VCDs than the Pandora instrument observing at 300° VAA. This interpretation is confirmed when considering MAX-DOAS data acquired at 266.5° and 340° VAA only, as shown in Fig. 2(b). As can be seen, the agreement is significantly improved with a slope of 0.92, a correlation coefficient of 0.93, a MD of -1.94×10^{15} molec .cm^{-2}, and a MRD of −19 %. Furthermore, Fig. 2(c), which compares the MAX-DOAS values averaged from 266.5° and 340°, demonstrates an even better agreement with a slope of 0.96, a correlation coefficient of 0.96, a MD of -1.62×10^{15} molec .cm^{-2}, and a MRD of −18 %.

Although aligning the VAA of both instruments improves the comparison results, Pandora results still show slightly lower tropospheric NO_2 VCDs than the MAX-DOAS columns. This discrepancy may

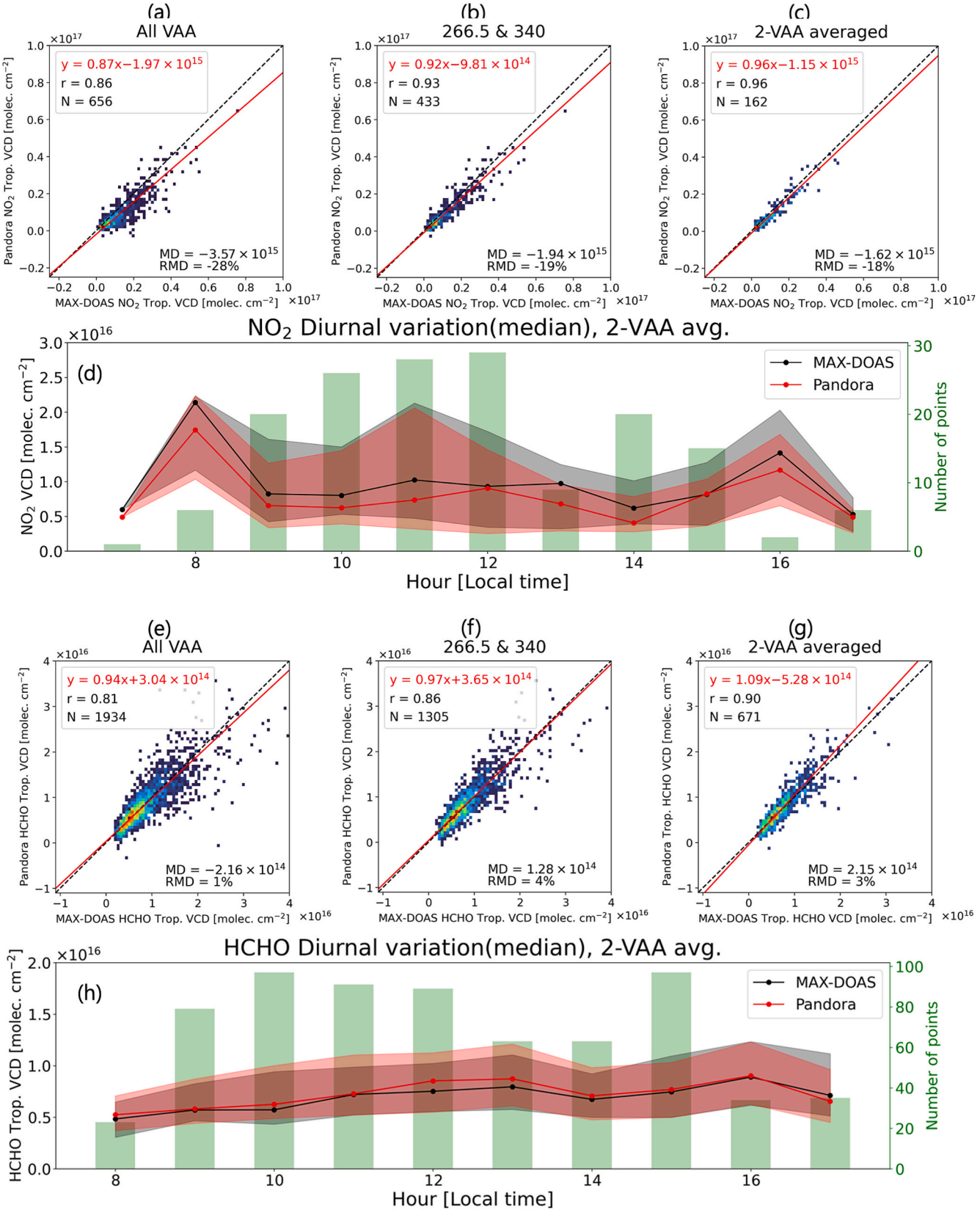

Fig. 2. Comparison of Pandora and MAX-DOAS tropospheric NO_2 VCD (panels a-d) and tropospheric HCHO VCD (panels e-h) in Incheon from July 2022 to November 2022. Panels (a) to (c) are scatter density plots between Pandora (y-axis) and MAX-DOAS (x-axis) of (a) all VAA, (b) 266.5° and 340°, and (c) 2-VAA averaged. Panel (d) is the diurnal variation of tropospheric NO_2 columns observed from 2-VAA averaged MAX-DOAS (black) and Pandora (red). The solid line depicts the median value, top and bottom of the shade are 25 and 75 percentiles of each instrument, and the green bar represents the number of coincident measurement points at each bin. Panels (e)-(h) are the same as (a)-(d), for tropospheric VCD of HCHO.

originate from algorithmic differences such as assumptions on aerosols, the a priori profile of NO_2, and the radiative transfer calculation. The MMF algorithm directly runs radiative transfer simulations by utilizing the VLIDORT (Spurr, 2006) model which allows for explicit treatment of light interactions with aerosols and trace gases. In contrast, the PGN algorithm employs a simplified approach where tropospheric vertical columns and profiles are derived from a set of simplified equations making use of O_4 dSCDs measured at a limited number of elevation angles (see Frieß et al., 2019, and the PGN documentation available online). The PGN algorithm uses spectra observed at elevation angles of 15°, 30°, and 90° (Cede and Tiefengraber, 2023) while the MMF processes spectra from more elevation angles (1°, 2°, 3°, 4°, 5°, 6°, 8°, 15°, 30°, and 90°). The inclusion of lower elevation angles enhances the sensitivity close to the surface. Although Pandora data show slightly lower tropospheric NO_2 columns, both instruments observe consistent diurnal variations, with double peaks at 8 and 16 LST, which correspond to rush hours.

The tropospheric HCHO VCD retrieved from Pandora sky measurements is currently distributed as an unvalidated product. Here, we compare it to the IUP-Bremen MAX-DOAS data to assess its accuracy and suitability for use as a reference for GEMS validation. Like for tropospheric NO_2, panels (e) and (g) from Fig. 2 show that aligning the VAA of MAX-DOAS and Pandora instruments also leads to a better agreement between the HCHO measurements. However, in comparison to NO_2, the alignment of the viewing geometry had a smaller impact on the agreement between Pandora and MAX-DOAS HCHO measurements. The slope changes from 0.94 to 1.09, and the correlation coefficient increases from 0.81 to 0.90. This suggests that while HCHO also exhibits spatial inhomogeneity, the magnitude is less pronounced than for NO_2. The diurnal pattern of HCHO in Incheon generally exhibits a monotonic increase throughout the day, with slight decreases observed around 14 and 17 LST. This pattern can be attributed to two key factors. First, HCHO is primarily formed through atmospheric photochemical reactions, which are enhanced by rising temperatures and solar shortwave radiation, leading to its typical behavior of having minimum levels in the early morning, increasing throughout the afternoon, and decreasing in the evening again. Second, the direct emissions from mobile sources can explain the increasing HCHO concentration. Considering the diurnal pattern of NO_2, high traffic volumes around 16 LST in Incheon likely contribute to the continued increase in HCHO levels, rather than a decrease. This pattern is similarly observed by both instruments.

The agreement found between Pandora and MAX-DOAS HCHO measurements is similar to the one obtained in previous studies comparing different MAX-DOAS instruments (Kreher et al., 2020; Pinardi et al., 2013; Tirpitz et al., 2021).

4.2. *Pandora direct-sun measurement vs MAX-DOAS*

Fig. 3(a) presents a comparison between the HCHO total columns (TCD) from Pandora direct-sun measurements and tropospheric HCHO VCD from the IUP-Bremen MAX-DOAS instrument. A good correlation is found between the two data sets with a correlation coefficient of 0.90,

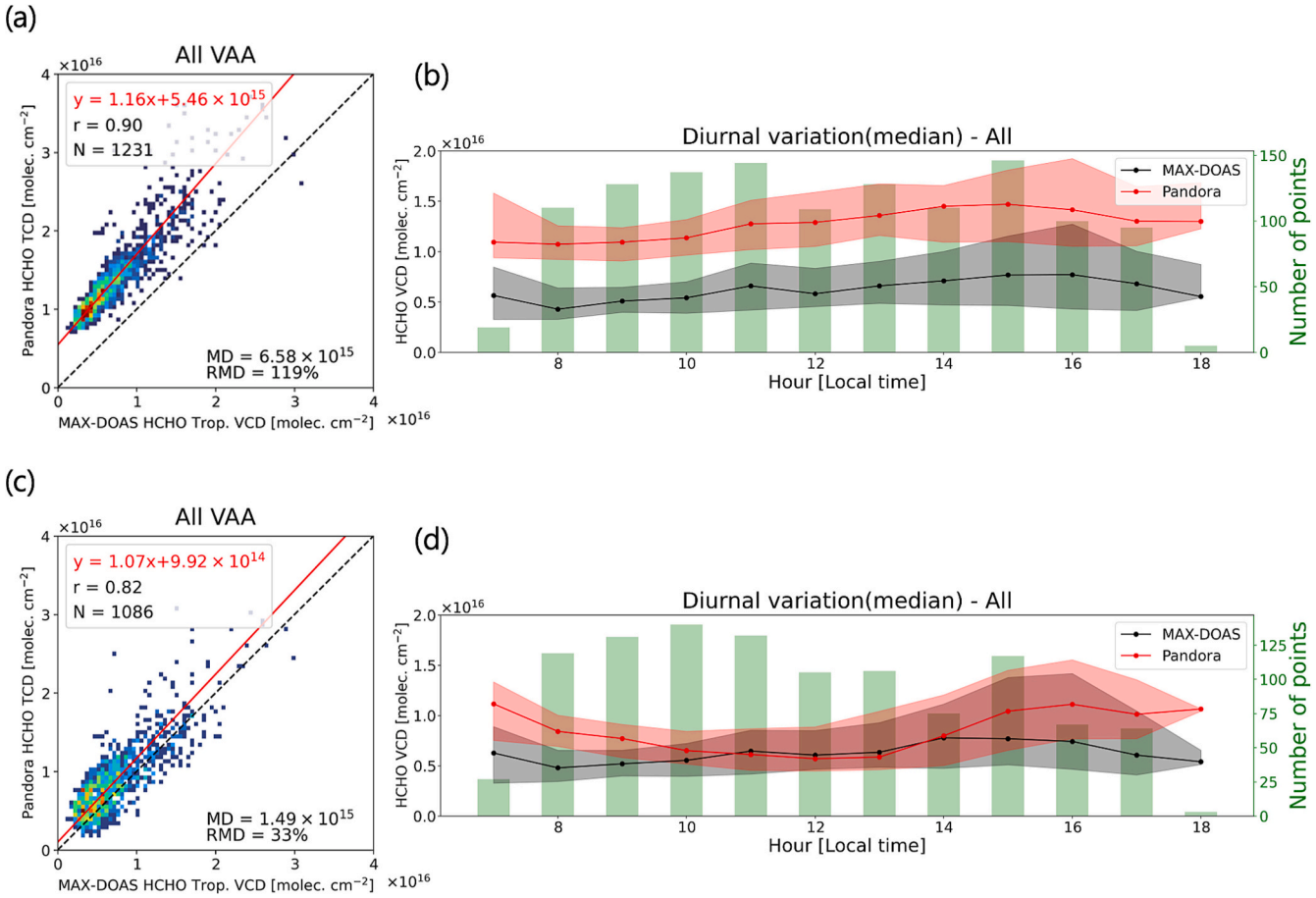

Fig. 3. Comparison results for Pandora direct-sun products (HCHO TCD) and MAX-DOAS (HCHO tropospheric VCD) in Incheon from July 2022 to November 2022. Panel (a) is a comparison of result between Pandora HCHO TCD and MAX-DOAS tropospheric HCHO VCD. Panel (b) shows the diurnal variation of the median column of MAX-DOAS (black) and Pandora (red). The top and bottom of the shade represent the 25th and 75th percentile of each instrument and the green bar is the number of coincident points. Pannel (c) and (d) are the same as (a) and (b), but with a different Pandora retrieval, using a 2nd order background polynomial in the spectral fitting.

however the Pandora HCHO TCDs are substantially larger compared to the MAX-DOAS tropospheric VCD HCHO with a slope of 1.16, a MD of 6.58 × 10^{15} molec. cm^{-2} and a MRD of 119 %. The MAX-DOAS measured the tropospheric HCHO VCD and Pandora direct-sun measurement provided HCHO total column, so it is expected that Pandora direct-sun data are larger than the simultaneous MAX-DOAS data. We examined data from the GEOS-Chem model and from the KORUS-AQ (Korea U.S.-Air Quality) field campaign (Herman et al., 2018) that reported HCHO vertical profiles up to 8 km measured by the Compact Atmospheric Multispecies Spectrometer (CAMS) (Richter et al., 2015), as well as HCHO profiles up to 5 km obtained from the DC-8 aircraft (Kwon et al., 2021). All these data show that the HCHO column above 4 km is small in comparison to the observed discrepancy between the Pandora direct-sun and MAX-DOAS observations. After consultation with the PGN team, a revised direct-sun data set was provided for P189. This version has a slightly modified spectral retrieval scheme where a 2nd order polynomial closure parameter is used instead of the usual 4th order one. This change was made because the instrumental spectral feature was biasing the 4th order background polynomial leading to a cross-correlation with the HCHO retrieval. By changing to a 2nd order polynomial, this bias was removed, but at the cost of a higher uncertainty. As a result of this change (see Figs. 3(c) and (d)) the MD decreased from 6.58 × 10^{15} molec. cm^{-2} to 1.49 × 10^{15} molec. cm^{-2} and the MRD from 119 % to 33 %. We note however that the change in retrieval settings also leads to an increase of the reported mean uncertainty from 9.83 × 10^{14} molec. cm^{-2} to 2.36 × 10^{15} molec. cm^{-2} (see Fig. A.3). In terms of the diurnal variation, shown in Fig. 3(d), the MAX-DOAS and the corrected Pandora data set show different diurnal patterns. The bias correction was most significant between 10 and 14 LST; thus, the corrected Pandora HCHO TCD shows U-shaped pattern with a local minimum at 13 LST, while the MAX-DOAS HCHO VCD shows a monotonic increase from 9 LST to 14 LST. Notably, in Fig. A.3 (b), the reported total uncertainty significantly increased between 10 and 15 LST, the period when the bias correction was most effective.

5. GEMS NO_2 and HCHO validation

5.1. Total column NO_2

In this section, we only focus on the evaluation of NO_2 TCDs from operational v2.0 algorithm. Note that Lange et al. (2024) evaluated the GEMS tropospheric NO_2 VCD product using the same MAX-DOAS stations as listed in Table 1.

For total column NO_2 validation, only GEMS pixels that contain the Pandora station are used to optimize the spatial coincidence between satellite and reference data. Pandora data are averaged within a ± 30 min window centered around the satellite scan time. Both GEMS and Pandora data are filtered with quality criteria as described in Section 3.

Fig. 4 presents the comparison of GEMS total column NO_2 at station P54 (Seoul) and P20 (Busan). The statistics for all Pandora stations in Korea are summarized in table A.1. Due to its larger urban scale and high anthropogenic NO_x emissions, Seoul generally shows higher NO_2 TCDs compared to Busan. GEMS captures well the typical seasonal cycle with higher values in winter and lower values in the summer season (Choi et al., 2021; Jang et al., 2017). Similar to the previous GEMS NO_2 VCD validation research by Kim et al. (2023), Edwards et al. (2024), and Lange et al. (2024), the statistical analysis indicates that GEMS overestimates the NO_2 VCD compared to both Pandora instruments (P54 and P20), with MD of 1.40 × 10^{16} molec. cm^{-2} and 2.85 × 10^{15} molec. cm^{-2}, and MRD of 68 % and 36 %, respectively. This overestimation is higher in winter. Notably, at P20, the Product Evaluation of GEMS L2 via Assessment with S5P and Other Sensors (PEGASOS) report (Eichmann et al., personal communication, 2024) also shows consistent results. However, for P20, there was a larger number of instances where GEMS observed smaller TCD than the Pandora instrument, with differences larger than 1 × 10^{15} molec. cm^{-2}. Nevertheless, in terms of correlation, GEMS and Pandora instruments (P54 and P20) show fair agreement with correlation coefficient of 0.76 and 0.65, respectively. Fig. A.4 shows the validation results of both GEMS and TROPOMI at coincident measurement times. In both stations, GEMS tends to also overestimate TROPOMI.

Fig. 4(d) and (h) shows the diurnal variation of NO_2 TCDs at P54 and P20 separated into weekdays and weekend. At P54 (Seoul), both Pandora and GEMS observe the same diurnal pattern during weekdays with an increase in the morning, a peak at noon, and a decrease in the afternoon. GEMS shows higher NO_2 TCDs compared to Pandora during the entire period, but the magnitude of the overestimation is significantly higher around noon. Furthermore, both show higher columns on weekdays. The difference between GEMS and Pandora VCDs is significantly larger during weekdays than during weekends. Additionally, as seen in Fig. 4(a), discrepancies between GEMS and P54 are smaller in summer but become more pronounced in winter and early spring. Since winter and early spring contribute a larger number of comparisons than summer, their influence on the diurnal variability shown in Fig. 4(c) and (d) is greater. This suggests that the seasonal bias is also reflected in the diurnal variation plots.

At the P20 site, the diurnal patterns of NO_2 TCDs observed by GEMS and Pandora differ. The diurnal pattern of the NO_2 TCD observed by GEMS at the P20 site is similar to the diurnal pattern observed by GEMS at the location of P54, exhibiting an inverted U shape with a peak at noontime, whereas the Pandora showed fairly constant NO_2 VCDs until 14 LST and an increase afterwards. The weekend/weekday analysis (see Fig. 4(h)) reveals that both Pandora and GEMS observe similar diurnal patterns on weekends, but differ on weekdays: Pandora observes a U-shaped pattern with the lowest value at noontime while GEMS observes a similar pattern as during weekends, leading to a discrepancy in diurnal patterns between GEMS and Pandora. We cannot conclude the exact cause of the discrepancy in diurnal patterns between GEMS and Pandora in Busan with the current observational data. However, NO_2 spatial inhomogeneity is suggested as a potential contributing factor. Judd et al. (2019) analyzed the impact of spatial resolution on comparisons between satellite data and Pandora using Geostationary Trace gas and Aerosol Sensor Optimization (GeoTASO) airborne measurements collected from May to June 2017 over the western shore of Lake Michigan and the Los Angeles Basin. Their results showed that the coarse spatial resolution of OMI (18 km × 18 km) was insufficient to capture the fine-scale spatial features within urban areas compared to the higher resolution of TROPOMI (5 km × 5 km). This study focused on large urban centers in the United States, smaller cities like Busan may require observation with even higher spatial resolution to address these challenges. Lange et al. (2024) investigated the diurnal pattern discrepancy between GEMS and Pandora in Busan by analyzing high-wind (≥3 m/s) and low-wind (<3 m/s) conditions separately. They found that under windy conditions, the Pandora captured an increase in NO_2 VCD during the late afternoon, whereas GEMS did not. This discrepancy may be attributed to local transport. This finding suggests that NO_2 hotspots occurring at spatial scales smaller than the satellite resolution can lead to discrepancies between satellite retrievals and Pandora observations. For observations at larger SZAs, AMFs are expected to be more uncertain. This uncertainty is further enhanced for larger aerosol loads and with low boundary layer heights in the morning and evening. Investigations are planned to explore this issue in more detail.

The validation results for all Pandora stations over Korea from October 2021 to November 2022 are shown in Fig. 5. Overall, the GEMS NO_2 TCD product tends to be larger than the Pandora observations over Korea, with a slope of 1.83, a correlation coefficient of 0.87, an MD of 7.39 × 10^{15} molec. cm^{-2}, and an MRD of 41 %. The SMA region (P189, P149, P54, indicated with red boxes in Fig. 5(b) and (c)) exhibits a larger magnitude of overestimation with an MD of 1.35 × 10^{16} molec. cm^{-2} and an MRD of 67 %, while non-SMA region stations (P20, P150, P164) show an MD of 1.85 × 10^{15} molec. cm^{-2} and an MRD of 17 %. The box-

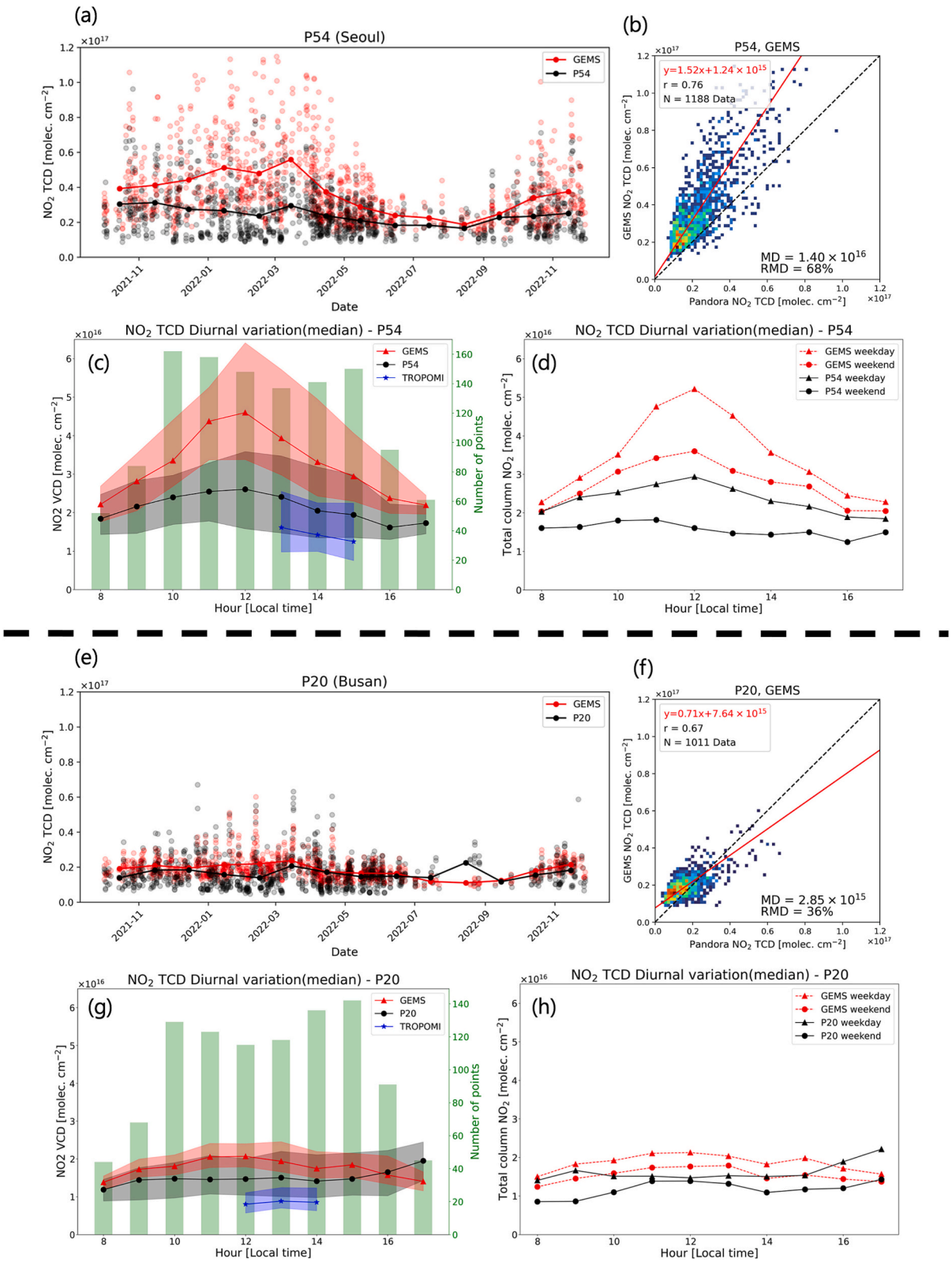

Fig. 4. Comparison of hourly GEMS total column NO_2 for P54 (panels a-d) and P20 (panels e-h). Black, red, and blue color indicate Pandora, GEMS, and TROPOMI data, respectively. Panel (a) and (e) are the timeseries of Pandora and GEMS observations. Transparent dots are hourly data and solid lines with solid dots represent the monthly averaged data. Panel (b) and (f) show the scatter density plot between Pandora (x-axis) and GEMS (y-axis) with RMA regression (red solid line). Panel (c) and (g) are the diurnal variation during the entire period. The shaded region covers the 25 to 75 percentiles of each instrument, and the gray bars represents the number of points at each hour (right hand axes). Panels (d) and (h) are diurnal variations of weekday (triangle) and weekend (circle) of GEMS (red) and Pandora (black).

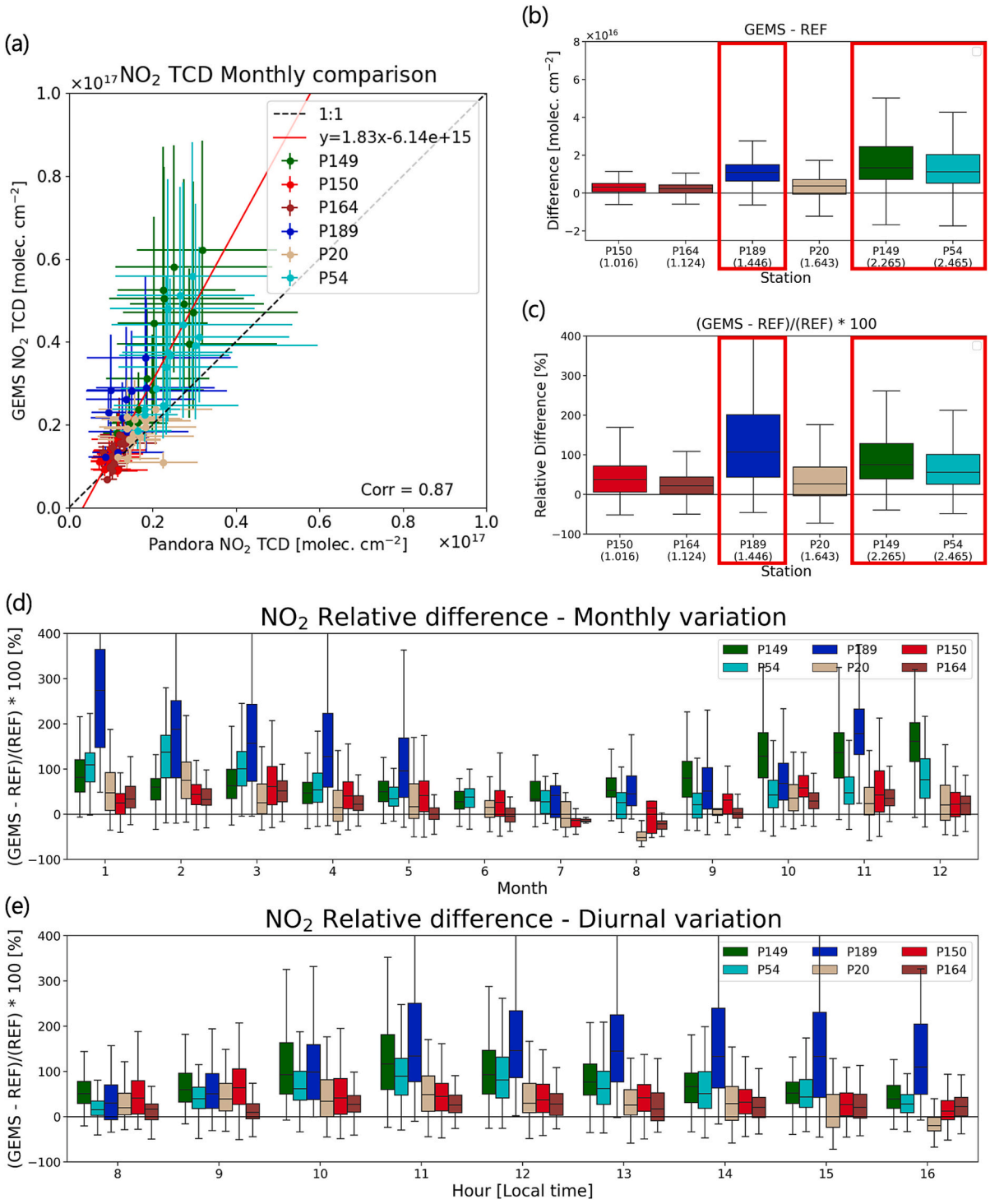

Fig. 5. Overall validation results of GEMS total column NO_2. (a) Scatter plot of monthly averaged total column NO_2 of GEMS and Pandora with error bars from 10th to 90th percentile. Box-whisker plot of (b) MD and (c) MRD. Stations are sorted by the mean value of Pandora as indicated below the station number in units of 10^{16} molec.cm^{-2} and the red boxes represent the SMA region instruments. Panel (d) and (e) are the box-whisker plot of monthly and diurnal variation of the MRD.

whisker plots of MRD in Fig. 5(d) and (e) demonstrate seasonal and diurnal variations of the MRD. The MRD shows the minimum in summer, and the maximum in winter, decreasing from March to August, which is followed by an increase. The MRD shows an additional diurnal variation, with a maximum around noon and being lowest in the morning and evening. It should be noted that this diurnal variation of MRD includes one year of data. Early morning and late afternoon data are mainly from the summer season, whereas data around noon represent all seasons (see Fig. A.2). Consequently, the observed diurnal pattern of MRD reflects a combination of real diurnal bias variation and bias variation caused by seasonal dependencies. Such overestimations can be mitigated through improvements in the AMF calculations. Lange et al. (2024) compared the GEMS operational NO_2 product with the scientific product retrieved by the IUP Bremen. The key differences regarding the AMF are the use of actual daily TM5 NO_2 vertical profile shapes, the replacement of the GEMS surface reflectivity product with TROPOMI Lambertian Equivalent Reflectivity (LER), and the use of SCIATRAN (Rozanov et al., 2014) instead of VLIDORT for radiative

transfer calculations. The overestimation was smaller in the scientific product compared to the operational product. The GEMS NO_2 IUP Bremen scientific product using the GEMS surface reflectivity product instead of the TROPOMI LER product, exhibits a larger bias compared to the scientific product retrieved using the TROPOMI LER.

5.2. Total column HCHO

The current operational GEMS HCHO v2.0 algorithm only provides the HCHO total columns. However, the bulk of HCHO is in the lower troposphere and to keep the continuity with previous studies by Kwon et al. (2019) and Lee et al. (2024), the tropospheric HCHO VCD obtained from both MAX-DOAS and sky measurements of Pandora instruments are used.

Due to the higher retrieval noise of HCHO compared to NO_2, we use the average value of the GEMS pixels withing a 10 km radius from each station for the validation of HCHO. Analogous to the NO_2 analysis, ground-based data are averaged within a ± 30 min window centered around the satellite scan time. TROPOMI tropospheric HCHO VCDs are also processed with the same method as used for the NO_2 validation.

Fig. 6 illustrates the validation results of the hourly GEMS HCHO product and the ground-based remote sensing instruments at UB_Incheon (MAX-DOAS; Incheon), and P150 (Pandora; Ulsan). In Fig. 6(a) and 6(e), GEMS effectively captures the typical seasonal variation of HCHO, with lower values in winter and higher values in summer, resulting from the enhancement of the VOCs oxidation and the increase in biogenic emissions driven by elevated temperature and solar shortwave radiation. The hourly comparison of GEMS with MAX-DOAS data at Incheon and with Pandora data at Ulsan (see Figs. 6(b) and 6(f) respectively), shows different results. Incheon MAX-DOAS data show a good agreement with GEMS with a slope of 0.83 and a correlation coefficient of 0.60, while P150 at Ulsan shows a slope of 0.59 and a correlation coefficient of 0.58. GEMS tends to underestimate high TCDs above 1×10^{16} molec. cm^{-2}, a behavior similar to the one observed with NO_2, and this occurs more frequently in Ulsan than in Incheon. If we overlap TROPOMI and GEMS validation results and only consider GEMS data at the TROPOMI overpass time (Fig. A.5), TROPOMI shows slightly lower correlation coefficients than GEMS but a higher regression slope.

In terms of diurnal variations, GEMS and ground-based instruments show similar patterns at each observation site with small differences in detail. In Incheon, Fig. 6(c), both GEMS and MAX-DOAS report a diurnal pattern of HCHO that remains flat until 15 LST, followed by an increase. However, GEMS shows lower values than MAX-DOAS before noontime. In Fig. 6(g), both GEMS and Pandora in Ulsan capture a similar diurnal pattern of decreasing HCHO VCDs in the morning followed by an increase in the afternoon. However, during 11 to 15 LST, while Pandora gradually increases, GEMS shows a parabolic increase with a local maximum at 13 LST. This discrepancy mainly originates from the autumn (SON) season, as can be seen in Fig. 6(h). As to the seasonal analysis, Incheon shows no significant seasonal difference in its diurnal pattern, only exhibiting HCHO TCDs that are lower in winter and higher in summer. In contrast, Ulsan shows notable differences in its diurnal variation patterns across seasons. In winter and autumn, the diurnal variation as measured by P150 is flat during the day, however GEMS data show an early afternoon peak, especially during autumn. In spring, the HCHO TCD, as measured by GEMS and P150, gradually increases throughout the day. In summer, both GEMS and Pandora exhibit a much steeper increase in VCD until 13 LST compared to other seasons. While Pandora maintains its peak VCD until 16 LST, GEMS shows a slight decrease after 13 LST and then a second peak at 16 LST. Since the P150 station is surrounded by mountains, the biogenic emission may cause this different diurnal pattern in the summer season. One potential reason for the differences in the detailed diurnal patterns observed between GEMS and ground-based remote sensing instruments could be related to background correction. The GEMS HCHO VCD is calculated by adding the background vertical column (VCD_0) from the CTM to the differential VCD (dVCD) retrieved from the observed radiance. According to Lee et al. (2024), the contribution of VCD_0 to the final VCD is approximately 70 % higher in GEMS compared to TROPOMI over Northeast Asia, including the Korean Peninsula. This indicates that the GEMS HCHO product relies more heavily on a priori data than TROPOMI. By managing the background correction issue in future updates, it is expected that GEMS will provide more accurate observations of the diurnal pattern of HCHO.

Fig. 7 shows the overall validation results from all MAX-DOAS and Pandora stations during the GMAP/SIJAQ campaign period. As reported by Lee et al. (2024), the correlation between the monthly averages of GEMS and both MAX-DOAS and Pandora data is good, with a correlation coefficient of 0.86 (for both) and a slope of 0.84 and 0.79 respectively. The MD and MRD compared with Pandora instruments were calculated as -5.35×10^{14} molec. cm^{-2} (-1.32×10^{15} molec. cm^{-2} to 8.02×10^{14} molec. cm^{-2}) and 18 % (−8 % to 59 %), respectively. Similarly, for all MAX-DOAS instruments, MD and MRD values were -2.57×10^{15} molec. cm^{-2} (-4.52×10^{15} molec. cm^{-2} to -1.05×10^{15} molec. cm^{-2}) and − 16 % (−40 % to 5 %). Considering the different MAX-DOAS instruments (see red box in Fig. 7(a)), validation results at BIRA and MPIC stations show significant negative difference suggesting that these instruments tend to report larger HCHO TCD than others. The larger negative bias observed at BIRA (Seoul and Suwon) and MPIC (Olympic) stations is attributed to instrumental and/or ground-based data retrieval issues rather than to GEMS-specific issues at these sites. A similar conclusion was reported in Van Roozendael et al. (2024). More work is needed to better understand the origin of these apparent discrepancies. Unlike for NO_2 validation results, there is no significant seasonal or diurnal variability in the MD and MRD for HCHO.

6. Conclusion

A comparison between MAX-DOAS and Pandora instruments in Incheon followed by a validation exercise of GEMS operational v2.0 NO_2 and HCHO total column products was conducted during the period October 2021 to November 2022, making use of the data from the GMAP and SIJAQ campaign data sets.

The comparison of tropospheric NO_2 and HCHO VCD between MAX-DOAS and the sky measurements from Pandora shows the importance of aligning the instruments viewing directions. Under aligned conditions, tropospheric NO_2 and HCHO VCDs retrieved from MAX-DOAS and Pandora instruments show good agreement. After proper matching of the viewing geometries, the slope and correlation coefficient increase from 0.87 to 0.96 and 0.86 to 0.96 for tropospheric NO_2 VCD. Similarly, the tropospheric HCHO VCD comparison shows a change in slope from 0.941 to 1.093, and an improvement in the correlation coefficient from 0.81 to 0.90.

The comparison of HCHO total columns from Pandora direct-sun measurements with HCHO tropospheric columns from MAX-DOAS measurements shows a significant discrepancy with a mean difference of 7.06×10^{15} molec. cm^{-2} and a relative mean difference ((Pandora-MAX-DOAS)/MAX-DOAS × 100 %) of 126 %. Revised data provided by the PGN team, using slightly modified retrieval settings, significantly reduces the bias compared to MAX-DOAS results. This correction led to an improvement of the MD and MRD from 7.06×10^{15} molec. cm^{-2} to 1.49×10^{15} molec. cm^{-2} and 126 % to 33 % respectively. However, this change is also accompanied by an increase of the reported uncertainty from 9.83×10^{14} molec. cm^{-2} to 2.35×10^{15} molec. cm^{-2}.

Pandora total column NO_2 products from 6 official PGN instruments over Korea were used for validation of GEMS operational v2.0 total column NO_2. Overall, GEMS shows a good agreement with the station, with a correlation coefficient of 0.87. However, GEMS tends to overestimate Pandora data, showing a slope of 1.83, and a mean relative difference of 41 %. Particularly the SMA region (P54, P149, P189) shows a large overestimation with a MRD of 67 % from GEMS compared to the other stations (P20, P150, P164). The magnitude of the overestimation

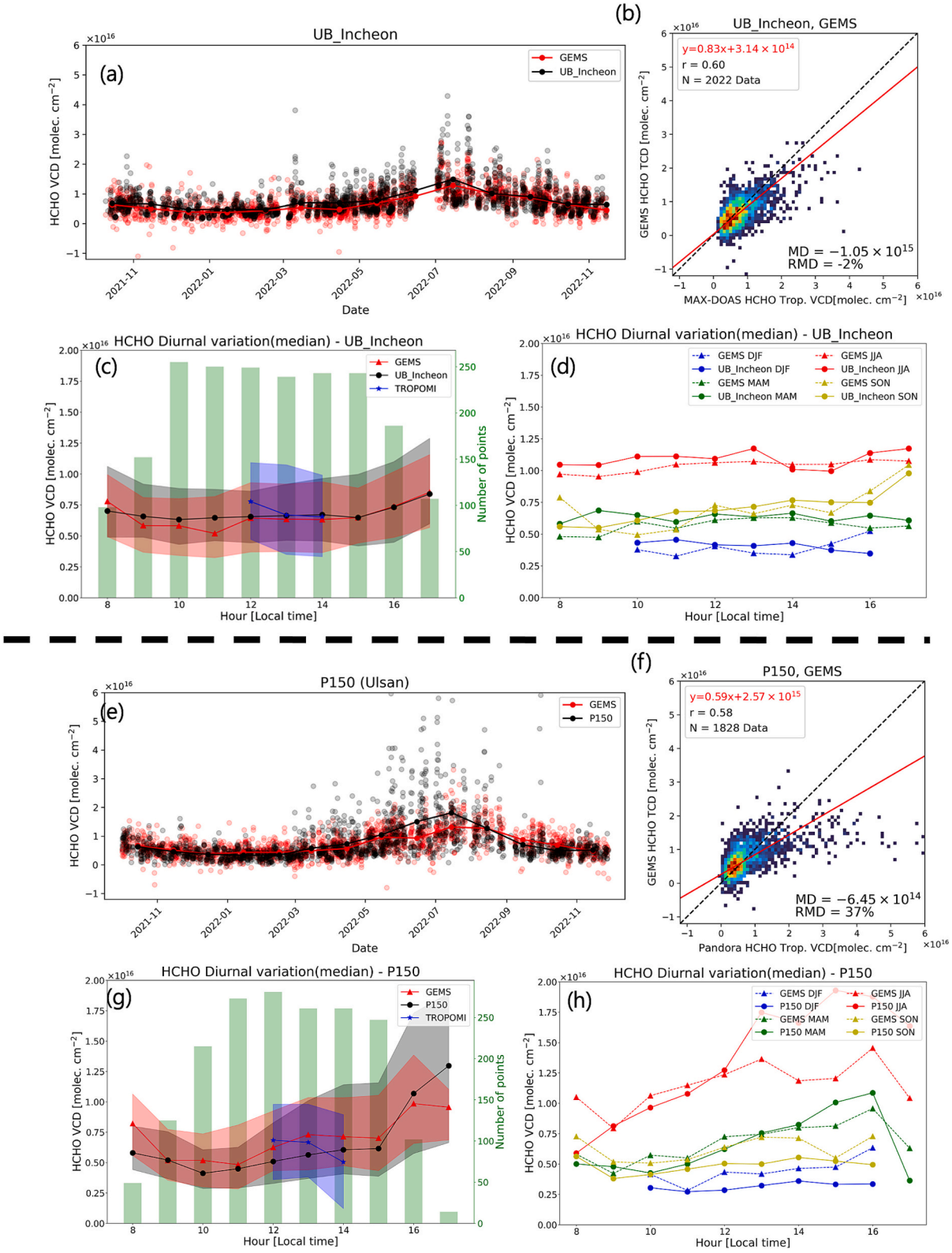

Fig. 6. Comparison of hourly HCHO TCD from GEMS and HCHO tropospheric VCD from ground-based remote sensing instruments at UB_Incheon (panels a-d) and P150 (panels e-h) station. Black, red, and blue color indicate ground-based instruments, GEMS, and TROPOMI data respectively. Panel (a) and (e) are the time series plots of ground-based instruments and GEMS. Transparent dots are hourly data and the solid line with solid dots represent the monthly averaged data. Panel (b) and (f) show the scatter density plot between ground-based instruments (x-axis) and GEMS (y-axis) with RMA regression (red solid line). Panel (c) and (g) show the diurnal variation from October 2021 to November 2022. The shaded regions represent the 25 and 75 percentiles of each instrument, and the gray bar is the number of points at each hour. Panel (d) and (h) are diurnal variations during each season (DJF: blue, MAM: green, JJA: red, SON: yellow), dashed-triangle for GEMS and solid-dots for the ground-based instruments.

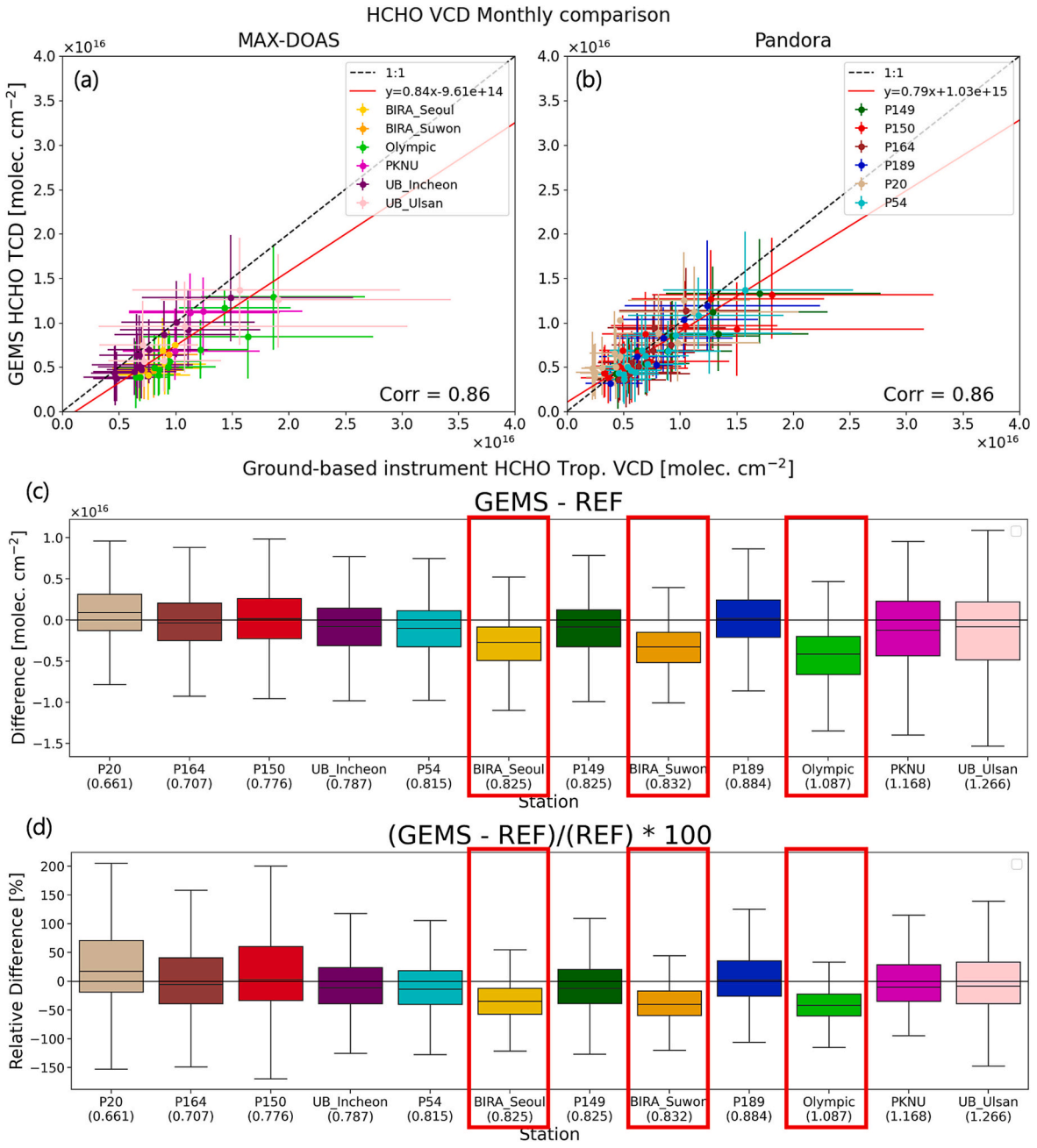

Fig. 7. Overall validation results of the GEMS HCHO product. The monthly scatter plot of averaged GEMS and MAX-DOAS (a) and Pandora (b) data. The black dashed line is 1:1 and the red solid line is the RMA regression line. Panel (c) and (d) are box-whisker plot of the MD and MRD of each station.

of GEMS is more pronounced in highly polluted conditions (i.e. during winter, and at noontime). Despite the reported overestimation, GEMS and Pandora data show similar diurnal patterns and seasonality. The exact cause of the overestimation remains unclear, further investigations are required to fully understand the underlying factors contributing to this discrepancy.

The validation of GEMS operational v2.0 HCHO total columns was conducted using HCHO data from 6 MAX-DOAS stations and 6 Pandora sky measurement. Overall, GEMS shows a good general agreement with both Pandora and MAX-DOAS data, with slopes of 0.84 and 0.80, respectively, and correlation coefficients of 0.86 in monthly averaged comparisons. Large columns, however, tend to be systematically underestimated. Furthermore, GEMS captures well the seasonal and diurnal variations of HCHO and does not display any significant pattern of MB and NMB.

Supplementary data to this article can be found online at https://doi.org/10.1016/j.scitotenv.2025.179190.

CRediT authorship contribution statement

Kangho Bae: Writing – review & editing, Writing – original draft, Visualization, Software, Methodology, Investigation, Formal analysis, Conceptualization. **Chang-Keun Song:** Writing – review & editing, Supervision, Resources. **Michel Van Roozendael:** Writing – review & editing, Resources, Investigation, Formal analysis. **Andreas Richter:** Writing – review & editing, Resources, Investigation. **Thomas Wagner:** Writing – review & editing, Resources, Investigation. **Alexis Merlaud:** Writing – review & editing, Investigation, Formal analysis. **Gaia Pinardi:** Writing – review & editing, Formal analysis. **Martina M. Friedrich:** Writing – review & editing, Investigation, Formal analysis,

Data curation. **Caroline Fayt:** Investigation, Data curation. **Ermioni Dimitropoulou:** Investigation. **Kezia Lange:** Writing – review & editing, Investigation. **Tim Bösch:** Writing – review & editing, Investigation. **Bianca Zilker:** Investigation. **Miriam Latsch:** Investigation. **Lisa K. Behrens:** Investigation. **Steffen Ziegler:** Investigation, Data curation. **Simona Ripperger-Lukosiunaite:** Investigation. **Leon Kuhn:** Writing – review & editing, Investigation. **Bianca Lauster:** Investigation. **Lucas Reischmann:** Investigation. **Katharina Uhlmannsiek:** Investigation. **Alexander Cede:** Validation, Data curation. **Martin Tiefengraber:** Writing – review & editing, Validation, Data curation. **Manuel Gebetsberger:** Validation, Data curation. **Rokjin J. Park:** Investigation, Data curation. **Hanlim Lee:** Investigation, Data curation. **Hyunkee Hong:** Resources, Project administration. **Lim-Seok Chang:** Resources, Project administration. **Kwonho Jeon:** Resources, Funding acquisition.

Declaration of competing interest

The authors declare that they have no known competing financial interests or personal relationships that could have appeared to influence the work reported in this paper.

Acknowledgements

This work was supported by grants from the Korea Environment Industry & Technology Institute (KEITI) through "Climate Change R&D Project for New Climate Regime" funded by the Korea Ministry of Environment (MOE) [Grant Number 2022003560002]; the National Institute of Environment Research (NIER) funded by the Ministry of Environment (MOE) of the Republic of Korea (Grant Number NIER-2021-03-03-007, NIER-2023-01-02-127, NIER-2024-03-02-006). We thank the National Institute of Environmental Research of South Korea for providing GEMS level-2 data and the organization of the GMAP2021 and SIJAQ2022 field campaigns. We thank all participants of the GMAP2021 and SIJAQ2022 field campaign. Copernicus Sentinel-5P level-2 NO_2 and HCHO data are used in this study. Sentinel-5 Precursor is a European Space Agency (ESA) mission on behalf of the European Commission. We thank to Ragi Rajagopalan, Stefanie Morhenn, Manuel Roca for calibrating and processing the Pandora data. We thank PGN instrument PIs, support staff and funding for establishing and maintaining the Pandora sites used in this investigation. The PGN is a bilateral project supported with funding from NASA and ESA.

Data availability

GEMS L2 NO_2 and HCHO data can be accessed at https://nesc.nier.go.kr/en/html/cntnts/91/static/page.do (National Institute of Environmental Research, NIER, last access: 13 August 2024). The TROPOMI NO_2 and HCHO data available at https://documentation.dataspace.copernicus.eu/Data/SentinelMissions/Sentinel5P.html (Copernicus dataspace, last access: 23 September 2024). The Pandora data are available from the PGN data archive (https://data.pandonia-global-network.org/, last access: 23 September 2024). The FRM_4DOAS MAX-DOAS data are available on request.

References

Behera, S.N., Sharma, M., 2011. Degradation of SO2, NO2 and NH3 leading to formation of secondary inorganic aerosols: an environmental chamber study. Atmos. Environ. 45, 4015–4024.
Beirle, S., Boersma, K.F., Platt, U., Lawrence, M.G., Wagner, T., 2011. Megacity emissions and lifetimes of nitrogen oxides probed from space. Science 333, 1737–1739.
Beirle, S., Dörner, S., donner S, Remmers J, Wang Y, Wagner T., 2019. The Mainz profile algorithm (MAPA). Atmospheric. Meas. Tech. 13, 1785–1806.
Bovensmann, H., Burrows, J., Buchwitz, M., Frerick, J., Noel, S., Rozanov, V., et al., 1999. SCIAMACHY: Mission objectives and measurement modes. J. Atmos. Sci. 56, 127–150.
Burrows, J.P., Weber, M., Buchwitz, M., Rozanov, V., Ladstätter-Weißenmayer, A., Richter, A., et al., 1999. The global ozone monitoring experiment (GOME): Mission concept and first scientific results. J. Atmos. Sci. 56, 151–175.
Cede, A., 2021. Manual for Blick Software Suite 1, 8.
Cede, A., Tiefengraber, M., 2023. Gebetsberger M. Lind ES, Pandonia Global Network Data Products Readme Document.
Chance, K., Palmer, P.I., Spurr, R.J., Martin, R.V., Kurosu, T.P., Jacob, D.J., 2000. Satellite observations of formaldehyde over North America from GOME. Geophys. Res. Lett. 27, 3461–3464.
Choi, Y., Kanaya, Y., Takashima, H., Irie, H., Park, K., Chong, J., 2021. Long-term variation in the tropospheric nitrogen dioxide vertical column density over Korea and Japan from the MAX-DOAS network, 2007–2017. Remote Sens. 13, 1937.
Chu, B., Ma, Q., Liu, J., Ma, J., Zhang, P., Chen, T., et al., 2020. Air pollutant correlations in China: secondary air pollutant responses to NO x and SO2 control. Environ. Sci. Technol. Lett. 7, 695–700.
Clarke, M., 1980. The reduced major axis of a bivariate sample. Biometrika 67, 441–446.
Crutzen, P.J., 1979. The role of NO and NO2 in the chemistry of the troposphere and stratosphere. Annu. Rev. Earth Planet. Sci. 7, 443–472.
Danckaert, T., Fayt, C., Van Roozendael, M., De Smedt, I., Letocart, V., Merlaud, A., et al., 2017. QDOAS Software User Manual.
de Foy, B., Lu, Z., Streets, D.G., Lamsal, L.N., Duncan, B.N., 2015. Estimates of power plant NOx emissions and lifetimes from OMI NO2 satellite retrievals. Atmos. Environ. 116, 1–11.
De Smedt, I., Müller, J.-F., Stavrakou, T., Van Der, A.R., Eskes, H., Van Roozendael, M., 2008. Twelve years of global observations of formaldehyde in the troposphere using GOME and SCIAMACHY sensors. Atmos. Chem. Phys. 8, 4947–4963.
De Smedt, I., Theys, N., Yu, H., Danckaert, T., Lerot, C., Compernolle, S., Van Roozendael, M., Richter, A., Hilboll, A., Peters, E., Pedergnana, M., Loyola, D., Beirle, S., Wagner, T., Eskes, H., van Geffen, J., Boersma, K.F., Veefkind, P., 2018. Algorithm theoretical baseline for formaldehyde retrievals from S5P TROPOMI and from the QA4ECV project. Atmos. Meas. Tech. 11 (4), 2395–2426.
De Smedt I, Romahn F, Eichmann K. S5P Mission Performance Centre Formaldehyde [L2_HCHO__] Readme. 2023: last acces: 18 March 2024.
Dimitropoulou, E., Hendrick, F., Pinardi, G., Friedrich, M.M., Merlaud, A., Tack, F., et al., 2020. Validation of TROPOMI tropospheric NO 2 columns using dual-scan multi-axis differential optical absorption spectroscopy (MAX-DOAS) measurements in Uccle. Brussels. Atmospheric Measurement Techniques 13, 5165–5191.
Dutta, C., Chatterjee, A., Jana, T., Mukherjee, A., Sen, S., 2010. Contribution from the primary and secondary sources to the atmospheric formaldehyde in Kolkata. India. Science of the total environment 408, 4744–4748.
Edwards, D.P., Martínez-Alonso, S., Jo, D.S., Ortega, I., Emmons, L.K., Orlando, J.J., et al., 2024. Quantifying the diurnal variation of atmospheric NO 2 from observations of the geostationary environment monitoring spectrometer (GEMS). EGUsphere 2024, 1–31.
Elsayed, N.M., 1994. Toxicity of nitrogen dioxide: an introduction. Toxicology 89, 161–174.
Eskes H, Eichmann K. S5P Mission Performance Centre Nitrogen Dioxide [L2_NO2__] Readme. 2023: last access: 18 March 2024.
Eum, K.-D., Honda, T.J., Wang, B., Kazemiparkouhi, F., Manjourides, J., Pun, V.C., et al., 2022. Long-term nitrogen dioxide exposure and cause-specific mortality in the US Medicare population. Environ. Res. 207, 112154.
Flynn, L. E., Seftor, C. J., Larsen, J. C., and Xu, P.: The Ozone Mapping and Profiler Suite, in: Earth Science Satellite Remote Sensing, edited by: Qu, J. J., Gao, W., Kafatos, M., Murphy, R. E., and Salomonson, V. V., Springer, Berlin, 279–296, doi:https://doi.org/10.1007/978-3-540-37293-6, 2006.
Friedrich, M.M., Rivera, C., Stremme, W., Ojeda, Z., Arellano, J., Bezanilla, A., et al., 2019. NO 2 vertical profiles and column densities from MAX-DOAS measurements in Mexico City. Atmos. Meas. Tech. 12, 2545–2565.
Frieß, U., Beirle, S., Alvarado Bonilla, L., Bösch, T., Friedrich, M.M., Hendrick, F., et al., 2019. Intercomparison of MAX-DOAS vertical profile retrieval algorithms: studies using synthetic data. Atmos. Meas. Tech. 12, 2155–2181.
Ghude, S.D., Fadnavis, S., Beig, G., Polade, S., Van Der, A.R., 2008. Detection of surface emission hot spots, trends, and seasonal cycle from satellite-retrieved NO2 over India. J. Geophys. Res. Atmos. 113.
González Abad, G., Vasilkov, A., Seftor, C., Liu, X., Chance, K., 2016. Smithsonian astrophysical observatory ozone mapping and profiler suite (SAO OMPS) formaldehyde retrieval. Atmos. Meas. Tech. 9, 2797–2812.
Gonzi, S., Palmer, P.I., Barkley, M.P., De Smedt, I., 2011. Van Roozendael M. Sensitivity to co-emitted aerosol and injection height. Geophysical Research Letters, Biomass burning emission estimates inferred from satellite column measurements of HCHO, p. 38.
Gulde S, Kolm M, Smith D, Maurer R, Courrèges-Lacoste GB, Sallusti M, et al. Sentinel 4: A geostationary imaging UVN spectrometer for air quality monitoring: Status of design, performance and development. International Conference on Space Optics—ICSO 2014. 10563. SPIE, 2017, pp. 1158–1166.
Haagen-Smit, A.J., 1952. Chemistry and physiology of Los Angeles smog. Ind. Eng. Chem. 44, 1342–1346.
Herman, J., Cede, A., Spinei, E., Mount, G., Tzortziou, M., Abuhassan, N., 2009. NO2 column amounts from ground-based Pandora and MFDOAS spectrometers using the direct-sun DOAS technique: Intercomparisons and application to OMI validation. J. Geophys. Res. Atmos. 114.
Herman, J., Spinei, E., Fried, A., Kim, J., Kim, J., Kim, W., et al., 2018. NO 2 and HCHO measurements in Korea from 2012 to 2016 from Pandora spectrometer instruments compared with OMI retrievals and with aircraft measurements during the KORUS-AQ campaign. Atmos. Meas. Tech. 11, 4583–4603.
Hönninger, G., Von Friedeburg, C., Platt, U., 2004. Multi axis differential optical absorption spectroscopy (MAX-DOAS). Atmos. Chem. Phys. 4, 231–254.

Irie, H., Takashima, H., Kanaya, Y., Boersma, K.F., Gast, L., Wittrock, F., et al., 2011. Eight-component retrievals from ground-based MAX-DOAS observations. Atmos. Meas. Tech. 4, 1027–1044.
Jaeglé, L., Steinberger, L., Martin, R.V., Chance, K., 2005. Global partitioning of NO x sources using satellite observations: relative roles of fossil fuel combustion, biomass burning and soil emissions. Faraday Discuss. 130, 407–423.
Jang, E., Do, W., Park, G., Kim, M., Yoo, E., 2017. Spatial and temporal variation of urban air pollutants and their concentrations in relation to meteorological conditions at four sites in Busan. South Korea. Atmospheric Pollution Research 8, 89–100.
Judd, L.M., Al-Saadi, J.A., Janz, S.J., Kowalewski, M.G., Pierce, R.B., Szykman, J.J., et al., 2019. Evaluating the impact of spatial resolution on tropospheric NO2 column comparisons within urban areas using high-resolution airborne data. Atmos. Meas. Tech. 12, 6091–6111.
Kim, J., Jeong, U., Ahn, M.-H., Kim, J.H., Park, R.J., Lee, H., et al., 2020. New era of air quality monitoring from space: geostationary environment monitoring spectrometer (GEMS). Bull. Am. Meteorol. Soc. 101, E1–E22.
Kim, S., Kim, D., Hong, H., Chang, L.-S., Lee, H., Kim, D.-R., et al., 2023. First-time comparison between NO 2 vertical columns from GEMS and Pandora measurements. Atmospheric Measurement Techniques Discussions 2023, 1–22.
Kim, S.W., Heckel, A., McKeen, S., Frost, G., Hsie, E.Y., Trainer, M., et al., 2006. Satellite-observed US power plant NOx emission reductions and their impact on air quality. Geophys. Res. Lett. 33.
Kousoulidou, M., Ntziachristos, L., Mellios, G., Samaras, Z., 2008. Road-transport emission projections to 2020 in European urban environments. Atmos. Environ. 42, 7465–7475.
Kreher, K., Van Roozendael, M., Hendrick, F., Apituley, A., Dimitropoulou, E., Frieß, U., et al., 2020. Intercomparison of NO 2, O 4, O 3 and HCHO slant column measurements by MAX-DOAS and zenith-sky UV–visible spectrometers during CINDI-2. Atmos. Meas. Tech. 13, 2169–2208.
Kwon, H.-A., Park, R.J., González Abad, G., Chance, K., Kurosu, T.P., Kim, J., et al., 2019. Description of a formaldehyde retrieval algorithm for the geostationary environment monitoring spectrometer (GEMS). Atmos. Meas. Tech. 12, 3551–3571.
Kwon, H.-A., Park, R.J., Oak, Y.J., Nowlan, C.R., Janz, S.J., Kowalewski, M.G., et al., 2021. Top-down estimates of anthropogenic VOC emissions in South Korea using formaldehyde vertical column densities from aircraft during the KORUS-AQ campaign. Elem Sci Anth 9, 00109.
Lange, K., Richter, A., Bösch, T., Zilker, B., Latsch, M., Behrens, L.K., et al., 2024. Validation of GEMS tropospheric NO2 columns and their diurnal variation with ground-based DOAS measurements. EGUsphere 2024, 1–42.
Laughner, J.L., Cohen, R.C., 2019. Direct observation of changing NO x lifetime in north American cities. Science 366, 723–727.
Lee, G.T., Park, R.J., Kwon, H.-A., Ha, E.S., Lee, S.D., Shin, S., et al., 2024. First evaluation of the GEMS formaldehyde retrieval algorithm against TROPOMI and ground-based column measurements during the in-orbit test period. Atmos. Chem. Phys. 24, 4733–4749.
Levelt, P.F., Van Den Oord, G.H., Dobber, M.R., Malkki, A., Visser, H., De Vries, J., et al., 2006. The ozone monitoring instrument. IEEE Trans. Geosci. Remote Sens. 44, 1093–1101.
Li, X., Rohrer, F., Brauers, T., Hofzumahaus, A., Lu, K., Shao, M., et al., 2014. Modeling of HCHO and CHOCHO at a semi-rural site in southern China during the PRIDE-PRD2006 campaign. Atmos. Chem. Phys. 14, 12291–12305.
Liu, O., Li, Z., Lin, Y., Fan, C., Zhang, Y., Li, K., et al., 2023. Evaluation of the first year of Pandora NO 2 measurements over Beijing and application to satellite validation. Atmospheric Measurement Techniques Discussions 2023, 1–32.
Lui, K., Ho, S.S.H., Louie, P.K., Chan, C., Lee, S., Hu, D., et al., 2017. Seasonal behavior of carbonyls and source characterization of formaldehyde (HCHO) in ambient air. Atmos. Environ. 152, 51–60.
Munro R, Eisinger M, Anderson C, Callies J, Corpaccioli E, Lang R, et al. GOME-2 on MetOp. Proc. of The 2006 EUMETSAT Meteorological Satellite Conference, Helsinki, Finland. 1216, 2006, pp. 48.
Ozgen, S., Cernuschi, S., Caserini, S., 2021. An overview of nitrogen oxides emissions from biomass combustion for domestic heat production. Renew. Sust. Energ. Rev. 135, 110113.
Park, J., Lee, H., Hong, H., 2020. Geostationary Environment Monitoring Spectrometer (GEMS) Algorithm Theoretical Basis Document NO2 Retrieval Algorithm.
Peters, E., Wittrock, F., Großmann, K., Frieß, U., Richter, A., Burrows, J., 2012. Formaldehyde and nitrogen dioxide over the remote western Pacific Ocean: SCIAMACHY and GOME-2 validation using ship-based MAX-DOAS observations. Atmos. Chem. Phys. 12, 11179–11197.
Pinardi, G., Van Roozendael, M., Abuhassan, N., Adams, C., Cede, A., Clémer, K., et al., 2013. MAX-DOAS formaldehyde slant column measurements during CINDI: intercomparison and analysis improvement. Atmos. Meas. Tech. 6, 167–185.
Pinardi, G., Van Roozendael, M., Hendrick, F., Theys, N., Abuhassan, N., Bais, A., et al., 2020. Validation of tropospheric NO2 column measurements of GOME-2A and OMI using MAX-DOAS and direct sun network observations. Atmospheric Masurement Techniques 13, 6141–6174.
Platt, U., Stutz, J., 2008. Differential Absorption Spectroscopy. Springer.
Richter, A., Burrows, J.P., Nüß, H., Granier, C., Niemeier, U., 2005. Increase in tropospheric nitrogen dioxide over China observed from space. Nature 437, 129–132.
Richter, D., Weibring, P., Walega, J.G., Fried, A., Spuler, S.M., Taubman, M.S., 2015. Compact highly sensitive multi-species airborne mid-IR spectrometer. Appl. Phys. B Lasers Opt. 119, 119–131.
Rozanov, V., Rozanov, A., Kokhanovsky, A.A., Burrows, J., 2014. Radiative transfer through terrestrial atmosphere and ocean: software package SCIATRAN. J. Quant. Spectrosc. Radiat. Transf. 133, 13–71.
Saw, G.K., Dey, S., Kaushal, H., Lal, K., 2021. Tracking NO2 emission from thermal power plants in North India using TROPOMI data. Atmos. Environ. 259, 118514.
Schiavon, M., Redivo, M., Antonacci, G., Rada, E.C., Ragazzi, M., Zardi, D., et al., 2015. Assessing the air quality impact of nitrogen oxides and benzene from road traffic and domestic heating and the associated cancer risk in an urban area of Verona (Italy). Atmos. Environ. 120, 234–243.
Schneider, P., Lahoz, W.A., van der A R., 2015. Recent satellite-based trends of tropospheric nitrogen dioxide over large urban agglomerations worldwide. Atmos. Chem. Phys. 15, 1205–1220.
Spinei, E., Whitehill, A., Fried, A., Tiefengraber, M., Knepp, T.N., Herndon, S., et al., 2018. The first evaluation of formaldehyde column observations by improved Pandora spectrometers during the KORUS-AQ field study. Atmos. Meas. Tech. 11, 4943–4961.
Spinei, E., Tiefengraber, M., Müller, M., Gebetsberger, M., Cede, A., Valin, L., Szykman, J., Whitehill, A., Kotsakis, A., Santos, F., Abbuhasan, N., Zhao, X., Fioletov, V., Lee, S.C., Swap, R., 2020. Effect of Polyoxymethylene (POM-H Delrin) offgassing within Pandora head sensor on direct sun and multi-axis formaldehyde column measurements in 2016–2019. Atmos. Meas. Tech. Discuss. 2020, 1–24.
Spurr, R.J., 2006. VLIDORT: A linearized pseudo-spherical vector discrete ordinate radiative transfer code for forward model and retrieval studies in multilayer multiple scattering media. J. Quant. Spectrosc. Radiat. Transf. 102, 316–342.
Technical Support Document EPA's 2011 National-scale Air Toxics Assessment, 2011 NATA TSD, 2015. United States Environmental Protection Agency, United States. https://www.epa.gov/sites/production/files/2015-12/documents/2011-nata-tsd.pdf.
Tirpitz, J.L., Frieß, U., Hendrick, F., Alberti, C., Allaart, M., Apituley, A., et al., 2021. Intercomparison of MAX-DOAS vertical profile retrieval algorithms: studies on field data from the CINDI-2 campaign. Atmos. Meas. Tech. 14, 1–35.
Tzortziou, M., Herman, J.R., Cede, A., Abuhassan, N., 2012. High precision, absolute total column ozone measurements from the Pandora spectrometer system: comparisons with data from a brewer double monochromator and Aura OMI. J. Geophys. Res. Atmos. 117.
Van Der, A.R., Eskes, H., Boersma, K., Van Noije, T., Van Roozendael, M., De Smedt, I., et al., 2008. Trends, seasonal variability and dominant NOx source derived from a ten year record of NO2 measured from space. J. Geophys. Res. Atmos. 113.
Van Der, A.R., Peters, D., Eskes, H., Boersma, K., Van Roozendael, M., De Smedt, I., et al., 2006. Detection of the trend and seasonal variation in tropospheric NO2 over China. J. Geophys. Res. Atmos. 111.
van Geffen, J.H.G.M., Eskes, H.J., Boersma, K.F., Veefkind, J.P., 2022. TROPOMI-ATBD of the Total and Tropospheric NO2 Data Products.
Van Roozendael, M., Hendrick, F., Friedrich, M.M., Fayt, C., Bais, A., Beirle, S., et al., 2024. Fiducial reference measurements for air quality monitoring using ground-based MAX-DOAS instruments (FRM4DOAS). Remote Sens. 16, 4523.
Veefkind, J.P., Aben, I., McMullan, K., Förster, H., De Vries, J., Otter, G., et al., 2012. TROPOMI on the ESA Sentinel-5 precursor: A GMES mission for global observations of the atmospheric composition for climate, air quality and ozone layer applications. Remote Sens. Environ. 120, 70–83.
Verhoelst, T., Compernolle, S., Pinardi, G., Lambert, J.-C., Eskes, H.J., Eichmann, K.-U., et al., 2021. Ground-based validation of the Copernicus sentinel-5p TROPOMI NO2 measurements with the NDACC ZSL-DOAS, MAX-DOAS and Pandonia global networks. Atmospheric. Meas. Tech. 14, 481–510.
Zhu, L., Jacob, D.J., Keutsch, F.N., Mickley, L.J., Scheffe, R., Strum, M., et al., 2017a. Formaldehyde (HCHO) as a hazardous air pollutant: mapping surface air concentrations from satellite and inferring cancer risks in the United States. Environ. Sci. Technol. 51, 5650–5657.
Zhu, L., Mickley, L.J., Jacob, D.J., Marais, E.A., Sheng, J., Hu, L., et al., 2017b. Long-term (2005–2014) trends in formaldehyde (HCHO) columns across North America as seen by the OMI satellite instrument: evidence of changing emissions of volatile organic compounds. Geophys. Res. Lett. 44, 7079–7086.
Zoogman, P., Liu, X., Suleiman, R., Pennington, W., Flittner, D., Al-Saadi, J., et al., 2017. Tropospheric emissions: monitoring of pollution (TEMPO). J. Quant. Spectrosc. Radiat. Transf. 186, 17–39.